NASA/TM-2002-212128

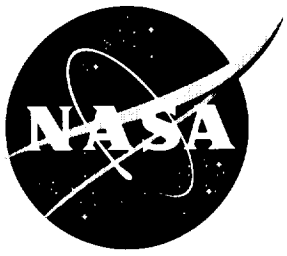

# Multirate Flutter Suppression System Design for the Benchmark Active Controls Technology Wing

## *Part I: Theory and Design Procedure*

*Gregory S. Mason and Martin C. Berg*
*University of Washington, Seattle, Washington*

*Vivek Mukhopadhyay*
*Langley Research Center, Hampton, Virginia*

December 2002

# The NASA STI Program Office . . . in Profile

Since its founding, NASA has been dedicated to the advancement of aeronautics and space science. The NASA Scientific and Technical Information (STI) Program Office plays a key part in helping NASA maintain this important role.

The NASA STI Program Office is operated by Langley Research Center, the lead center for NASA's scientific and technical information. The NASA STI Program Office provides access to the NASA STI Database, the largest collection of aeronautical and space science STI in the world. The Program Office is also NASA's institutional mechanism for disseminating the results of its research and development activities. These results are published by NASA in the NASA STI Report Series, which includes the following report types:

- TECHNICAL PUBLICATION. Reports of completed research or a major significant phase of research that present the results of NASA programs and include extensive data or theoretical analysis. Includes compilations of significant scientific and technical data and information deemed to be of continuing reference value. NASA counterpart of peer-reviewed formal professional papers, but having less stringent limitations on manuscript length and extent of graphic presentations.

- TECHNICAL MEMORANDUM. Scientific and technical findings that are preliminary or of specialized interest, e.g., quick release reports, working papers, and bibliographies that contain minimal annotation. Does not contain extensive analysis.

- CONTRACTOR REPORT. Scientific and technical findings by NASA-sponsored contractors and grantees.

- CONFERENCE PUBLICATION. Collected papers from scientific and technical conferences, symposia, seminars, or other meetings sponsored or co-sponsored by NASA.

- SPECIAL PUBLICATION. Scientific, technical, or historical information from NASA programs, projects, and missions, often concerned with subjects having substantial public interest.

- TECHNICAL TRANSLATION. English-language translations of foreign scientific and technical material pertinent to NASA's mission.

Specialized services that complement the STI Program Office's diverse offerings include creating custom thesauri, building customized databases, organizing and publishing research results ... even providing videos.

For more information about the NASA STI Program Office, see the following:

- Access the NASA STI Program Home Page at ***http://www.sti.nasa.gov***

- E-mail your question via the Internet to help@sti.nasa.gov

- Fax your question to the NASA STI Help Desk at (301) 621-0134

- Phone the NASA STI Help Desk at (301) 621-0390

- Write to:
  NASA STI Help Desk
  NASA Center for AeroSpace Information
  7121 Standard Drive
  Hanover, MD 21076-1320

NASA/TM-2002-212128

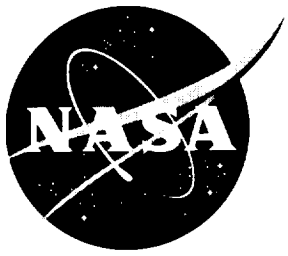

# Multirate Flutter Suppression System Design for the Benchmark Active Controls Technology Wing

## *Part I: Theory and Design Procedure*

*Gregory S. Mason and Martin C. Berg*
*University of Washington, Seattle, Washington*

*Vivek Mukhopadhyay*
*Langley Research Center, Hampton, Virginia*

National Aeronautics and
Space Administration

Langley Research Center
Hampton, Virginia 23681-2199

December 2002

Available from:

NASA Center for AeroSpace Information (CASI)
7121 Standard Drive
Hanover, MD 21076-1320
(301) 621-0390

National Technical Information Service (NTIS)
5285 Port Royal Road
Springfield, VA 22161-2171
(703) 605-6000

# CONTENTS

# 1. INTRODUCTION

To study the effectiveness of various control system design methodologies, the NASA Langley Research Center initiated the Benchmark Active Controls Project. In this project, the various methodologies will be applied to design a flutter suppression systems for the *Benchmark Active Controls Technology* (BACT)Wing (also called the PAPA wing). Eventually, the designs will be implemented in hardware and tested on the BACT wing in a wind tunnel.

This report describes a project at the University of Washington to design a *multirate* flutter suppression system for the BACT wing. The objective of the project was two fold. First, to develop a methodology for designing robust multirate compensators, and second, to demonstrate the methodology by applying it to the design of a multirate flutter suppression system for the BACT wing.

The contributions of this project are

1) Development of an algorithm for synthesizing robust low order multirate control laws. The algorithm is capable of synthesizing a single compensator which stabilizes both the nominal plant and multiple plant perturbations.
2) Development of a multirate design methodology, and supporting software, for modeling, analyzing and synthesizing multirate compensators.
3) Design of a multirate flutter suppression system for NASA's BACT wing which satisfies the specified design criteria

Blank

# 2. A METHODOLOGY FOR DESIGNING MULTIRATE COMPENSATORS

## 2.1. OVERVIEW

Our design methodology defines the general approach a designer would take, and provides the specific tools needed, to solve a multirate control problem. The general approach dictated by the methodology is to model a multirate system as an equivalent single-rate system, to synthesize the compensator using parameter optimization, and to analyze the resulting closed-loop system by applying modified single-rate techniques to a single-rate equivalent model of the multirate system. A schematic of our multirate design methodology is shown in Fig. 2.1. In the following paragraphs we first introduce the terminology and notation unique to multirate systems and then discuss each aspect of the design methodology along with the applicable design and analysis tools.

## 2.2. DEFINITIONS, ASSUMPTIONS AND NOTATION

A multirate sampled-data system consists of a continuous plant in feedback with a multirate compensator. A block diagram of such a system is shown in Fig. 2.2 where the signals $y_s$ and $y_c$ are continuous output vectors, $u$ is the continuous control input vector, $w$ is the continuous process noise, and $v$ is the discrete sensor noise. The primary components of the multirate system are the continuous plant, the sampling hardware (e.g. A/D converters), a digital processor (e.g., a computer), and the signal holding hardware (e.g., zero-order-hold D/A converters). The samplers, digital processor and holds will be referred to together as the "multirate compensator". We will assume that the plant is linear time-invariant, and that the multirate compensator conforms to the Generalized Multirate Control Law Structure discussed in Section 2.3.1.

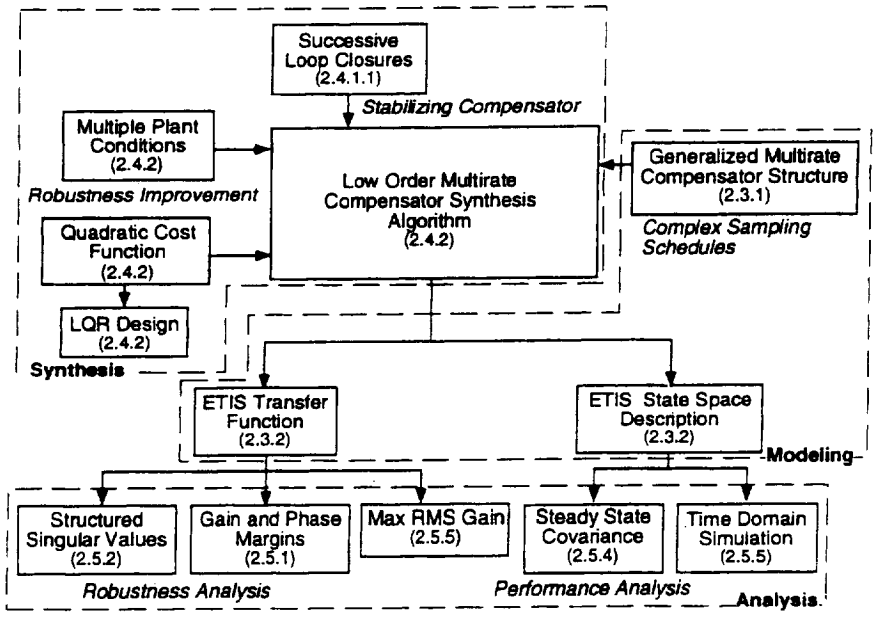


Figure 2.1. A multirate design methodology. Section numbers indicated in parentheses

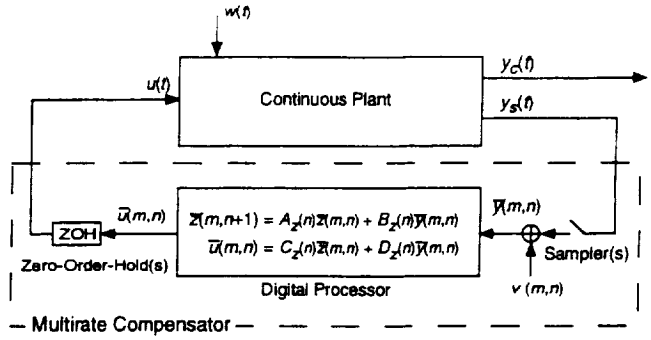


Figure 2.2. Multirate sampled-data system

As we will later see, multirate systems which satisfy our assumptions are periodically time-varying. To emphasize their periodic nature we will use a double index notation for the independent variable of a sampled or discrete signal. For example, given a continuous signal $y(t)$, $y(m,n)$ represents $y(t)$ sampled at the time $t = (mN + n)T$; where the integer $N$ is the period of repetition; $T$ is the sampling period; $m$ =0, 1, ... ; and $n$=0, 1, ... $N$-1.

The design methodology presented in the following sections provides tools to model the closed loop system in Fig. 2.2, to compute optimum values of $A_z$, $B_z$, $C_z$ and $D_z$, and to analyze the performance of the closed-loop system.

## 2.3. MODELING A MULTIRATE SYSTEM

Two useful modeling tools are the Generalized Multirate Control Law Structure (GMCLS) and the Equivalent Time-Invariant System (ETIS).

### 2.3.1. The GMCLS

The GMCLS is a control law structure which describes a multirate compensator of arbitrary dynamic order, with an independent sampling rate for every compensator input, and independent update rates for every processor state and compensator output. A multirate compensator with the GMCLS is shown in Fig. 2.2. In this figure each element of the continuous plant output $y_s$ is sampled at an independent rate. The sampled value of $y_s$, $\bar{y}$, is combined with the current processor state vector, $\bar{z}$, using the state space structure shown in the figure. Each element of the processor state vector, $\bar{z}$, is updated at an independent rate. The continuous output from the compensator, represented by the vector $u$, is formed by holding the output from the digital processor, $\bar{u}$, with a zero-order-hold. Each element of the vector $\bar{u}$ can be held at an independent rate to form $u$.

Conceptually, one can divide the multirate compensator into two parts, the "sampling schedule" and the digital processor gains. This is the approach used in the GMCLS. The "sampling schedule" is a description of when each compensator input is sampled and when each compensator output and processor state is updated, while the digital processor gains determine the dynamics of the digital processor.

#### *2.3.1.1. Sampling Schedule for a GMCLS*

In general, the sampling and updating of the elements of $y_s$, $\bar{z}$, and $\bar{u}$ in Fig. 2.2 can occur at any time. However, to conform to the GMCLS, we require that these sample and update activities occur only at integer multiples of some fixed time, called the *shortest time period* (STP). The actual value of the STP is arbitrary, but it is often a function of the hardware and software used to implement the control law. We also require that the sampling and updating activities of the sensors, states and outputs repeat themselves after some fixed period of

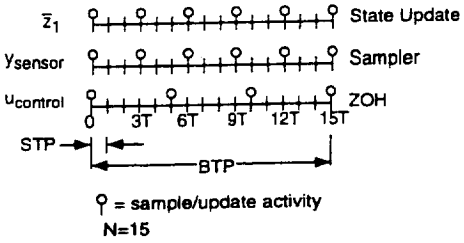


Figure 2.3 Example Sampling Schedule

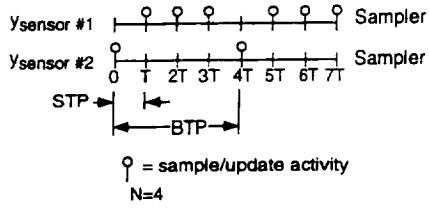


Figure 2.4 Aperiodic Sampling Schedule

time. (This requirement disallows, for example, a system whose sampling period is a function of the time require to execute the control software which might vary with control inputs values.) The period of repetition of the sampling schedule is called the *basic time period* (BTP). Finally, we define

$$\text{the integer } N = \frac{\text{BTP}}{\text{STP}} \quad \text{and the value} \quad T = \text{STP} \tag{2.1}$$

In our double index notation, the first index ($m$) in, for example, $y(m,n)$ indicates the integer number of BTP's which have elapsed when the sample/update occurred and the second index ($n$) indicates the integer number of STP's which have elapsed within the current BTP when the sample/update occurred.

We can represent the sampling schedule for the multirate compensator graphically, as shown in Fig. 2.3. The figure shows a time line for each sampler, processor state, and zero-order-hold. The time line is divided into one STP increments. On the left side of the time line is a description of the signal or state being sampled or updated. On the right side is a description of the particular activity represented by the time line, e.g., state update, sampler, or zero-order-hold. Circles on each time line indicate when a sample or update activity associated with that particular signal or state takes place. Usually the sampling schedule is shown for only one BTP since the sampling schedule repeats itself every BTP.

In most applications, the sampling/updating activities for a given sensor, output or state will be periodic *within* the BTP, as is shown in Fig. 2.3. However, the sampling/updating activities do not have to be periodic within the BTP. The only requirement is that the sampling/updating activities have some period of repetition (the BTP) and that they occur at integer multiples of the STP. Once the STP and BTP have been selected, the designer can arbitrarily specify sampling/updating activities at any multiple of the STP within one BTP. An example of a multirate sampling schedule in which the sampling/updating activities are not periodic within the BTP is shown in Fig. 2.4. A sampling policy like this might be used to multiplex multiple inputs through a single analog to digital converter.

*2.3.1.2. Digital Processor Gains*

The processor gains are the values of the matrices $A_z$, $B_z$, $C_z$, and $D_z$ in Fig. 2.2. Like the sampling schedule, they can be periodically time-varying with a period of repetition of one BTP. Generally, these matrices are free design parameters which can be adjusted by the designer to improve the performance of the multirate compensator. The synthesis algorithm discussed in Section 2.4 can be used to calculate optimum values for these gains.

*2.3.1.3. State Space Formulation of the GMCLS*

A compensator with the GMCLS can be modeled as a periodically time-varying discrete-time system. The state space form of the GMCLS is given by

$$z(m,n+1) = A_g(n)z(m,n) + B_g(n)y(m,n) \tag{2.2a}$$

$$u(m,n) = C_g(n)z(m,n) + D_g(n)z(m,n) \tag{2.2b}$$

where

$$z(m,n) = [\bar{z}(m,n)^T \;\; \bar{y}(m,n)^T \;\; \tilde{u}(m,n)^T]^T \tag{2.3}$$

and $\tilde{u}(m,n)$ is used to model the sample and hold activity from $\bar{u}(m,n)$ to $u(m,n)$. The form of $A_g$, $B_g$, $C_g$ and $D_g$ is given in [Berg, Mason & Yang 1991] and [Mason & Berg 1992] which are included as Attachments 1 and 2.

We should emphasize that Eqn. (2.2) is used to model the *complete* sampling/updating activities and dynamics of a multirate compensator. It would not be used in the actual implementation of the compensator. When implemented, the sample and hold activities of the inputs and outputs would be performed by appropriate hardware. The only dynamics to be calculated are those associated with the processor state vector $\bar{z}$.

*2.3.1.4. Factored Form of the GMCLS*

Equation (2.2) is a convenient form to model the general multirate compensator. The difficulty with Eqn. (2.2) is that it ties up the digital processor matrices, $A_z(n)$, $B_z(n)$, $C_z(n)$, and $D_z(n)$, in the model matrices $A_g(n)$, $B_g(n)$, $C_g(n)$, and $D_g(n)$. The matrices $A_z(n)$, $B_z(n)$, $C_z(n)$, and $D_z(n)$, which describe the dynamics of the digital processor, are the unknown design parameters which we will later optimize. We can separate the processor dynamics matrices from the model matrices as follows.

Define the composite compensator matrix:

$$P(n) = \begin{bmatrix} D_g(n) & C_g(n) \\ B_g(n) & A_g(n) \end{bmatrix} \tag{2.4}$$

and factor $P(n)$ as follows

$$P(n) = S_1(n)P_z(n)S_2(n) + S_3(n) \tag{2.5}$$

$$\text{where } P_z(n) = \begin{bmatrix} D_z(n) & C_z(n) \\ B_z(n) & A_z(n) \end{bmatrix} \tag{2.6}$$

and $S_1$, $S_2$ and $S_3$ are the switching matrices defined by the sampling schedule for the compensator. Their exact form is given in [Mason 1992] and [Mason & Berg 1992]

It is important to note the difference between $P(n)$ and $P_z(n)$ in Eqn. (2.5). $P(n)$ is a periodically time-varying matrix defined by Eqn. (2.4). It includes all the information about the processor gains *and* the sampling/update schedule. $P_z(n)$ contains *only* the gains for the processor dynamics and is independent of the sampling schedule.

*2.3.1.5. Implementation*

The Generalized Multirate Control Law Structure (GMCLS) provides a framework for dealing with multiple sample/update rates, time delays, and periodically time-varying gains in a digital control system. It gives the designer freedom to either select the "sampling schedule" that best solves the problem, or if necessary, to use the "sampling schedule" dictated by existing hardware and software, with out having to worry about the bookkeeping involved with multiple rates and time delays.

In practice, the GMCLS is implemented in software and is rarely used directly by the designer. The designer need only supply the sampling schedule and values for the digital processor gains to provide a complete compensator description. This description can then be transformed directly into a single-rate periodically time-varying system using the GMCLS.

The GMCLS is used extensively by the synthesis algorithm described in Section 2.4, and by the modeling and analysis software referred to in Section 2.5. Documentation for this software is provided in Ref. 43.

### 2.3.2. The Equivalent Time-Invariant System (ETIS)

A multirate compensator with the periodically time-varying structure discussed in Section 2.3.1.3 can be further transformed into a single-rate *Equivalent Time-Invariant System* (ETIS) with the form shown below

$$x(m+1,0) = A_E\, x(m,0) + B_E\, u_E(m,0) \tag{2.7a}$$

$$y_E(m,0) = C_E\, x(m,0) + D_E\, u_E(m,0) \tag{2.7b}$$

where

$$y_E(m,0) = \begin{bmatrix} y_s(m,0) \\ y_s(m,1) \\ \vdots \\ y_s(m,N\text{-}1) \end{bmatrix} \quad \text{and} \quad u_E(m,0) = \begin{bmatrix} u(m,0) \\ u(m,1) \\ \vdots \\ u(m,N\text{-}1) \end{bmatrix} \tag{2.8}$$

We use the subscript $E$ to denote vectors and matrices strictly associated with the ETIS. See [Meyer & Burrus 1975] or [Mason 1992] for a definition of $A_E$, $B_E$, $C_E$ and $D_E$.

A key feature of an ETIS is that a multirate, or periodically time-varying system will be stable if and only if its ETIS is stable [Kono 1971]. Also notice that the ETIS input/output vectors are composite vectors containing the input/output values of the multirate (or periodically-time varying) system at $N$ sampling times. Consequently, an ETIS is always MIMO even if the original system is SISO. If the multirate system has $p$ inputs, $q$ outputs and a sampling period of one STP then the ETIS is a single-rate linear time-invariant system with $N\,p$ inputs, $N\,q$ outputs and a sampling period of one BTP.

#### *2.3.2.1. Implementation*

The ETIS is fundamental to the analysis of multirate systems. It allows one to evaluate the performance and stability of complex systems comprised of multirate, periodically time-varying and/or single-rate components using only techniques developed for linear time-invariant single-rate systems. For example, to evaluate the stability of the system in Fig. 2.2, we would first transform the multirate compensator into its ETIS with a given value for $N$. Then we would discretize the plant at the STP of the compensator using a zero-order-hold and transform the resulting single-rate system into an ETIS using the BTP of the compensator. Next, the plant and compensator ETIS's could be combined in feedback just as if they were traditional single-rate systems. Finally, we could determine the stability of the original multirate sampled-data system from the eigenvalues of its closed-loop ETIS.

Documentation for software capable of transforming multirate and single-rate systems into their ETIS's is provided in Ref. 43 (NASA TM 2002-212129)

## 2.4. SYNTHESIZING A MULTIRATE COMPENSATOR

When designing a multirate compensator for the system in Fig. 2.2 there are three components one must consider: the compensator structure (this includes the dynamical order of the digital processor), the sampling schedule, and the values for the digital processor gains. In our design methodology the compensator structure and sampling schedule are selected by the designer based on the open-loop plant dynamics, the hardware constraints, if any, and the desired closed-loop performance. Values for the digital processor gains are

calculated by our synthesis algorithm so as to provide optimum closed-loop performance for the chosen compensator structure and sampling schedule. In the following paragraphs we discuss compensator structure and sampling schedule selection, and provide a brief description of our synthesis algorithm. A complete discussion of the algorithm is provided in Ref. 43 (NASATM 2002-212129).

### 2.4.1. Compensator Structure and Sampling Schedule Selection

The choice of compensator structure and sampling schedule is problem dependent. It depends on the hardware constraints, the open-loop plant dynamics, and the design objectives. Two often used multirate compensator structures are worthy of mention, however. They are successive loop closure and coupled successive loop closures. (Also see [Berg 1986] for a discussion of successive loop closures.)

#### *2.4.1.1. Successive Loop Closures Structure*

The simplest multirate compensator structure is successive loop closures (SLC). This structure consists of multiple decoupled single-rate control loops, each loop operating at a unique sample/update rate. The state space representation of a SLC structure with two loops is

$$\begin{Bmatrix} x_{fast}(m+1) \\ x_{slow}(n+1) \end{Bmatrix} = \begin{bmatrix} a_{fast} & 0 \\ 0 & a_{slow} \end{bmatrix} \begin{Bmatrix} x_{fast}(m) \\ x_{slow}(n) \end{Bmatrix} + \begin{bmatrix} b_{fast} & 0 \\ 0 & b_{slow} \end{bmatrix} \begin{Bmatrix} y_{fast}(m) \\ y_{slow}(n) \end{Bmatrix} \tag{2.9a}$$

$$\begin{Bmatrix} u_{fast}(m) \\ u_{slow}(n) \end{Bmatrix} = \begin{bmatrix} c_{fast} & 0 \\ 0 & c_{slow} \end{bmatrix} \begin{Bmatrix} x_{fast}(m) \\ x_{slow}(n) \end{Bmatrix} + \begin{bmatrix} d_{fast} & 0 \\ 0 & d_{slow} \end{bmatrix} \begin{Bmatrix} y_{fast}(m) \\ y_{slow}(n) \end{Bmatrix} \tag{2.9b}$$

where $y$ represents the sampled input from the sensor and $u$ is the output to the zero-order-hold. The subscripts *fast* and *slow* denote inputs, outputs and states which are sampled/updated at a fast or slow rate, respectively.

SLC is best applied to control problems where the *closed-loop* dynamics are comprised of some fast and some slow dynamics with the bandwidths of the two separated by at least a factor of four. In this type of problem, the "fast" loop(s) of the SLC compensator, operating at a fast sampling/update rate, would be used to control the high bandwidth dynamics, while the "slow" loop(s), operating at a slower sampling/update rate, would be used to control the low bandwidth dynamics. Problems such as these usually fall into one of two categories.

In the first, the *open-loop* system exhibits both fast and slow dynamics. The multirate compensator is used to improve the performance of this system without drastically changing the fast or slow bandwidths. An example of this type of problem is an aircraft yaw damper/modal suppression system. The aircraft is open-loop stable and has some fast dynamics associated with the flexibility of the airframe and some slower dynamics associated with the yawing motion of the entire aircraft. A multirate compensator for such a system might consist of a high bandwidth loop to damp the airframe vibrations and a low bandwidth loop to improve yaw damping.

In the second type, the open-loop dynamics of the plant are arbitrary, but in feedback with the compensator the closed-loop system exhibits the characteristic fast and slow dynamics. These systems usually have a decoupled structure where sets of open-loop modes are strongly controllable and observable with a particular set of inputs and outputs and weakly controllable and observable with the remaining inputs and outputs. An example of this type of system is the two link robot arm (TLA) used in [Berg, Amit & Powell 1988], and in [Yang 1988]. All four of the open-loop poles of the TLA are at the origin of the "$s$" plane. The plant has two inputs and two outputs. Only two of the modes can be controlled with any one input. Similarly, only two of these modes can be observed with any one output. In the multirate design, one input/output pair is used to place

two of the closed-loop poles at a high frequency and the other input/output pair is used to place the other two closed-loop poles at a low frequency.

Sample rate selection for the individual control loops of a SLC design follows the same guide lines used in single-rate sample rate compensator design: the sample rate for each SLC loop should be 5 to 20 times faster than the closed-loop bandwidth desired for that loop. See [Franklin Powell & Workman 1990] for a discussion of sample rate selection for single-rate systems.

*2.4.1.2. Coupled Successive Loop Closures Structure*

The coupled SLC structure is the same as the traditional SLC structure except the designer can include cross feed terms which couple the fast and slow inputs and outputs of the design. In the state space formulation, cross coupling is represented by non-zero off diagonal terms in the compensator gain matrices. An example of a compensator structure with cross feed from the slow sampled sensor to the fast sampled/updated control loop is given in Eqn. (2.10).

$$\begin{Bmatrix} x_{fast}(m+1) \\ x_{slow}(n+1) \end{Bmatrix} = \begin{bmatrix} a_{fast} & 0 \\ 0 & a_{slow} \end{bmatrix} \begin{Bmatrix} x_{fast}(m) \\ x_{slow}(n) \end{Bmatrix} + \begin{bmatrix} b_{fast} & b_{fs} \\ 0 & b_{slow} \end{bmatrix} \begin{Bmatrix} y_{fast}(m) \\ y_{slow}(n) \end{Bmatrix} \tag{2.10a}$$

$$\begin{Bmatrix} u_{fast}(m) \\ u_{slow}(n) \end{Bmatrix} = \begin{bmatrix} c_{fast} & 0 \\ 0 & c_{slow} \end{bmatrix} \begin{Bmatrix} x_{fast}(m) \\ x_{slow}(n) \end{Bmatrix} + \begin{bmatrix} d_{fast} & d_{fs} \\ 0 & d_{slow} \end{bmatrix} \begin{Bmatrix} y_{fast}(m) \\ y_{slow}(n) \end{Bmatrix} \tag{2.10b}$$

This structure is best applied to systems which have coupling between their fast and slow closed-loop dynamics. See [Yang 1988] for a discussion of cross feed in the TLA problem.

### 2.4.2. Optimizing the Digital Processor Gains

Having chosen an appropriate compensator structure and sampling schedule, the designer can use our synthesis algorithm to calculate optimum values for the digital processor gains $A_Z$, $B_Z$, $C_Z$ and $D_Z$ such that the closed-loop system in Fig. 2.2 minimizes a quadratic cost function.

The primary design parameter for the synthesis algorithm is the quadratic cost function. By selecting an appropriate cost function, the designer can influence the performance of the resulting closed-loop system. The cost function minimized by our synthesis algorithm has the form

$$\bar{J} = \lim_{t\to\infty} E\left\{ \begin{bmatrix} y_C^T(t) & u^T(t) \end{bmatrix} \begin{bmatrix} Q_1 & M \\ M^T & Q_2 \end{bmatrix} \begin{bmatrix} y_C(t) \\ u(t) \end{bmatrix} \right\} \tag{2.11}$$

where $\bar{J}$ is the cost associated with the closed-loop system shown in Fig. 2.2. The vector $y_C$ is the continuous criterion output and $u$ is the continuous control input. $Q_1$, $Q_2$ and $M$ are the cost function weighting matrices and are free design parameters.

The cost function in Eqn. (2.11) has the same form in a continuous time LQR design. Thus the cost associated with the optimized multirate compensator and that of an LQR design can be compared directly. The designer can also use this fact to help select appropriate values for $Q_1$, $Q_2$ and $M$.

To improve the robustness of the compensator, the synthesis algorithm can optimize the digital processor gains for multiple plant conditions simultaneously. The resulting compensator will stabilize the each plant condition and provide overall optimum performance. This is accomplished by minimizing the new cost function of Eqn. (2.12) which is the sum of the costs associated with each plant condition.

$$J = \sum_{i=1}^{\mathbf{Np}} \bar{J}_i = \sum_{i=1}^{\mathbf{Np}} \lim_{t\to\infty} E\left\{ \begin{bmatrix} y_{ci}^T(t) & u_i^T(t) \end{bmatrix} \begin{bmatrix} Q_i & M_i \\ M_i^T & R_i \end{bmatrix} \begin{bmatrix} y_{ci}(t) \\ u_i(t) \end{bmatrix} \right\} \tag{2.12}$$

Here $\bar{J}_i$ is the cost associated with the $i^{th}$ plant perturbation and there are Np plant perturbations.

Optimum values of $A_z$, $B_z$, $C_z$, and $D_z$, occur when

$$\frac{\partial J}{\partial A_z} = 0, \ \frac{\partial J}{\partial B_z} = 0, \ \frac{\partial J}{\partial C_z} = 0, \text{ and } \frac{\partial J}{\partial D_z} = 0 \text{ or equivalently when } \frac{\partial J}{\partial P_z} = 0 \tag{2.13}$$

Our algorithm uses a gradient type numerical search and a closed form expression for the gradients in Eqn. (2.13) to determine values of the digital processor gains such that the conditions in Eqn. (2.13) are satisfied. Refer to [Mason & Berg 1992] in Attachment 1 for a closed form expression for the gradients in Eqn. 2.13. The synthesis software uses an iterative process to determine optimum values for the digital processor gains and the user must provide the software with an initial guess for $A_z$, $B_z$, $C_z$, and $D_z$. The initial guess must stabilize every plant condition considered in Eqn. (2.12).

### 2.4.3. Implementation

In practice, the steps for designing a compensator with our methodology are

1) Construct a continuous LQ regulator for each plant condition which achieves the desired performance for that condition.

2) Based on the desired closed-loop dynamics and the constraints imposed by the system hardware, choose an appropriate compensator structure and sampling schedule.

3) Using the chosen sampling schedule and compensator structure, design a compensator which stabilizes all plant perturbations. When the desired compensator structure is one of the two structures discussed in the previous section, the designer can use successive loop closures to find a stabilizing value for the digital processor gains. In successive loop closures, the plant is stabilized by closing one loop at a time, from one set of inputs to one set of outputs. To obtain a multirate compensator, each loop is closed using a different sampling/update rate. When, due either to a complex sampling schedule, or the complexities of the control problem, successive loop closures cannot be used to find a stabilizing value for the digital processor gains, use Yang's algorithm (see [Yang 1988]). This may seem counterproductive at first, since one of the reasons for developing our algorithm was the computational inefficiencies of Yang's algorithm. However, our experience has shown that, in general, Yang's algorithm converges to a stabilizing compensator fairly rapidly. It is the computation time associated with optimization of this stabilizing solution that tends to be excessive.

4) Calculate optimum values for the digital processor gains using the synthesis algorithm of Section 2.4.2. The cost function weighting matrices for the optimization are the same as those used to design the LQ regulators in Step 1. The starting point for the optimization is the stabilizing compensator designed in Step 3.

See Attachment 4 for the complete documentation of the software that implements the synthesis algorithm.

## 2.5. ANALYZING A MULTIRATE SYSTEM

Multirate system analysis is difficult because the periodic nature of a multirate system implies that a traditional transfer function does not exist. Thus, common analysis tools such as frequency response or Nyquist diagrams are not directly applicable to multirate systems. Our solution is to transform the multirate system into a linear time-invariant single-rate system, the ETIS, and then apply established single-rate analysis techniques using the Z-Transform of the ETIS. (Note: we write the Z-Transform of an ETIS where $N$=BTP/STP as $G_E(z^N)$.) The following paragraphs discuss five useful tools for analyzing the performance and stability of a multirate system based on its ETIS.

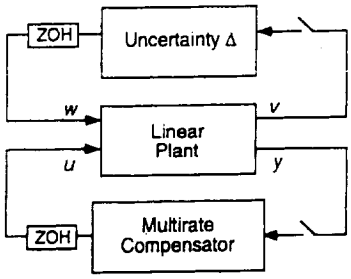


Figure 2.5. Plant/compensator configuration

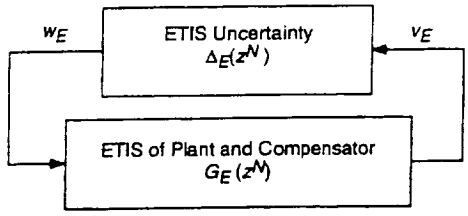


Figure 2.6. Plant/compensator with uncertainty

### 2.5.1. Gain and Phase Margins

In Section 2.3.2 we noted that a multirate system will be stable if and only if its ETIS is stable. Therefore, we can determine whether the multirate system is stable by applying the Nyquist criterion to its ETIS. Since all but trivial ETIS's are MIMO, we must use the multiloop Nyquist stability criterion. The multivariable Nyquist is a plot of the eigenvalues of the ETIS loop transfer function as the discrete variable $z$ traverses the unit circle [MacFarlane 1970] [Maciejowske 1990].

When the multirate system is SISO we can obtain traditional gain and phase margins from the multiloop Nyquist plot. Let $G_E(z^N)$ be the ETIS loop transfer function and let $\Delta$ be some constant gain and phase uncertainty at the plant input. If

$$\Delta(z) = k e^{j\theta} \text{ where } k e^{j\theta} \text{ is a scalar} \tag{2.14}$$

$$\text{then } \Delta_E(z^N) = I k e^{j\theta} \tag{2.15}$$

where $I$ is and $N \times N$ identity matrix

Now the new loop transfer function with the gain and phase uncertainty of Eqn. (2.15) can be written as

$$H_E(z^N)_{\text{loop}} = G_E(z^N) k e^{j\theta} \tag{2.16}$$

The multiloop Nyquist plot of $H_E(z^N)_{\text{loop}}$ is just the multiloop Nyquist plot of $G_E(z^N)$ scaled by the gain $k$ and rotated by the phase shift $\theta$ - the same as in traditional SISO Nyquist plots. Gain and phase margins for the multirate system can therefore be obtained from the multiloop Nyquist plot of $G_E(z^N)$ by determining the values of $k$ and $\theta$ which destabilize the ETIS. (See [Thompson 1986] for an alternate derivation using Kranc operators.)

When the multirate system is MIMO, the gain and phase margins calculated by this procedure apply simultaneously to all inputs and outputs, and are consequently not realistic measures of robustness. To obtain realistic measures of robustness for a MIMO multirate system, a norm based approach such as singular value analysis is required.

### 2.5.2. Singular Values

Singular values are useful for measuring the robustness of MIMO multirate systems. The key step in multirate singular value analysis is transforming the multirate system in Fig. 2.5 into an ETIS system which has the output feedback form shown in Fig. 2.6. Since the multirate system will be stable if and only if its ETIS is stable, the closed-loop system in Fig. 2.5 will be stable for a given value of $\Delta$ provided the closed-loop system in Fig. 2.6 is stable for a corresponding value of $\Delta_E$. Thus we can use single-rate techniques to evaluate the robustness of the ETIS system and relate those results directly to the associated multirate system.

*2.5.2.1. Unstructured Singular Value Analysis*

A bound on the smallest value of $\bar{\sigma}(\Delta_E)$ for which $\Delta_E$ destabilizes the system shown in Fig. 2.6 can be calculated using unstructured singular value analysis. This system will be stable for all $\Delta_E$ such that

$$\bar{\sigma}(\Delta_E(z^N)) < \frac{1}{\bar{\sigma}(G_E(z^N))} \quad \text{for all } z \text{ on the unit circle} \tag{2.17}$$

(see [Maciejowski 1989]). This result, however, is only a measure of the size of the smallest destabilizing $\Delta_E$ and is generally not a measure of the size of the smallest destabilizing uncertainty $\Delta$. Because the input/output vectors of an ETIS are composite vectors, containing the input/output values of the multirate system at $N$ sample times, $\Delta_E$ can be a complex function of the values of $\Delta$ at $N$ sample times. (The relation between $\Delta_E$ and $\Delta$ is given by Eqn. 2.7.) The size of the smallest destabilizing $\Delta_E$ found using unstructured singular value analysis is only a conservative estimate of the size of the smallest destabilizing $\Delta$. This estimate accounts for not only the fictitious perturbations normally associated with unstructured singular values, but also for time-varying and non-causal perturbations.

Consider the simple case where $\Delta$ is a constant. From Fig. 2.5 we have that

$$w = \Delta v \tag{2.18}$$

For an ETIS with $N$=2

$$w_E = \Delta_E v_E \quad \text{or} \quad \begin{Bmatrix} w(m,0) \\ w(m,1) \end{Bmatrix} = \begin{bmatrix} \Delta_{11} & \Delta_{12} \\ \Delta_{21} & \Delta_{22} \end{bmatrix} \begin{Bmatrix} v(m,0) \\ v(m,1) \end{Bmatrix} \tag{2.19}$$

A destabilizing $\Delta_E$ determined by singular value analysis might, for example, include block diagonal elements in $\Delta_E$ which are unequal, e.g. $\Delta_{11} \neq \Delta_{22}$. This corresponds to a time-varying perturbation because the gain between $w$ and $v$ varies with time. Another such $\Delta_E$ could include non-zero upper block diagonal elements in $\Delta_E$, e.g. $\Delta_{12} \neq 0$. This corresponds to a non-causal perturbation because a future input, $v(m,1)$, can affect the current output $w(m,0)$.

We can eliminate this conservativeness by restricting the allowable perturbations in $\Delta_E$. This leads directly to structured singular value analysis.

*2.5.2.2. Structured Singular Value Analysis*

In order for the ETIS uncertainty $\Delta_E$ to represent the actual uncertainty $\Delta$, its structure must obey Eqn. (2.7). Finding the size of the smallest destabilizing $\Delta_E$ subject to Eqn. (2.7) requires the solution of a structured singular value problem. For the system in Fig. 2.6 we define the structured singular value, $\mu$, as

$$\mu(G_E(z^N)) = \begin{cases} 0 \text{ if } \det(I - G_E(z^N)\Delta_E(z^N)) \neq 0 \text{ for all } \Delta \in \Delta_{BD} \\ \left( \min_{\Delta \in \Delta_{BD}} [\bar{\sigma}(\Delta(z))] \text{ such that } \det(I - G_E(z^N)\Delta_E(z^N)) = 0 \right)^{-1} \text{ otherwise} \end{cases} \tag{2.20}$$

where $\Delta_{BD}$ is the form of the permissible block diagonal perturbations $\Delta$ and the structure of $\Delta_E$ must satisfy Eqn. (2.7). The size of the smallest destabilizing perturbation $\bar{\sigma}(\Delta_{min})$ satisfies

$$\frac{1}{\bar{\sigma}(\Delta_{min})} = \sup_{\phi} \mu(G_E(z^N)) \quad \text{where } z^N = e^{j\phi} \tag{2.21}$$

For a discussion of $\mu$ and $\Delta_{BD}$ see [Doyle 1982].

Unfortunately, even a simply structured dynamic uncertainty $\Delta(z)$ transforms to an ETIS uncertainty, $\Delta_E(z^N)$, with a complex structure. For example, if $N$=2 then the ETIS of $\Delta(z)$ is

$$\Delta_E(z^2) = \frac{1}{2}\begin{bmatrix} \Delta(z)+\Delta(-z) & z^{-1}(\Delta(z)-\Delta(-z)) \\ z(\Delta(z)-\Delta(-z)) & \Delta(z)+\Delta(-z) \end{bmatrix} \tag{2.22}$$

In order to find the value of $\bar{\sigma}(\Delta_{\min})$ using Eqn. (2.21), one must solve Eqn. (2.20) with $\Delta_E$ constrained to have the structure in Eqn. (2.7). Currently there is no general technique for solving this problem. When, however, the uncertainty, $\Delta$, is a constant, as is the case for many problems, the ETIS uncertainty, $\Delta_E$, is also a constant with a repeated block diagonal form.

$$\Delta_E = diag(\Delta, \Delta, ..., \Delta) \text{ with } N \text{ blocks.} \tag{2.23}$$

There are several good methods for estimating $\bar{\sigma}(\Delta_{\min})$ when $\Delta_E$ has this block diagonal structure. One simple method for estimating $\mu$ when $\Delta$ is *strictly* diagonal is derived in [Safonov 1982]. It is

$$\mu(G_N(z^N)) \le \inf_D(\bar{\sigma}(\text{abs}(DG_N(z^N)D^{-1})) = \lambda_p(G_N(z^N)) \tag{2.24}$$

where abs($A$) is a matrix such that $[\text{abs}(A)]_{ij} = |A_{ij}|$; $A_{ij}$ is the $i^t j^{th}$ element of $A$; and $\lambda_p$ is the Perron-Frobenius eigenvalue.

*2.5.4.3 Implementation*

The procedure for performing singular value analysis via the ETIS is as follows

1) Transform the problem into the form shown in Fig. 2.5
2) Discretize the plant at the STP of the compensator and compute the ETIS of the plant using the $N$ of the compensator
3) Combine the ETIS of the plant and compensator to obtain the closed-loop system shown in Fig. 2.6
4) Use any applicable single-rate singular-value based analysis tool to compute the size of the smallest destabilizing uncertainty $\Delta_E$.
5) Interpret the results in the light of the fact that the computed results are for an ETIS uncertainty $\Delta_E$ whereas the actual plant uncertainty is $\Delta$. $\Delta_E$ is a function of $\Delta$ as given by Eqn. 2.7 and so the results might be conservative unless structured singular value analysis is used.

### 2.5.3. Maximum RMS Gain

The maximum RMS gain of a SISO *single-rate* system is the maximum gain on that system's Bode plot. As already noted, a traditional Bode plot cannot be generated for a *multirate* system. However, the maximum RMS gain of a SISO *multirate* system can be computed; it is the $H_\infty$ norm of the ETIS transfer function. This value, shown in Eqn. (2.25), plays the same role as the maximum Bode plot gain of a *single-rate* system.

$$\sup_{\text{RMS}(u)\neq 0} \frac{\text{RMS}(y(m,n))}{\text{RMS}(u(m,n))} = \sup_{\text{RMS}(u_E)\neq 0} \frac{\text{RMS}(y_E(m,0))}{\text{RMS}(u_E(m,0))} = \|G_E(z^N)\|_\infty \tag{2.25}$$

Actually, Eqn. (2.25) can be used to calculate the RMS gain of SISO or MIMO systems. It simply states that the maximum RMS gain of a transfer function $G_E$ is equivalent to the $H_\infty$ norm of $G_E$. See also the related work of [Sivashankar & Khargonekar 1991].

Unlike linear time invariant single-rate systems, the discrete input signal resulting in the maximum multirate RMS gain does not necessarily have the simple form $\sin(\omega T m)$. Instead it is comprised of the sum of

sinusoids of several distinct frequencies. Details on computing the signal of maximum RMS gain for a multirate system are given in [Mason & Berg 1992]

*2.5.3.1 Implementation*

One simple method for determining the $H_\infty$ norm is to plot the maximum singular value of $G_E$ as $z$ traverses the unit circle. $H_\infty(G_E)$ is then the peak value on that plot.

It is important to remember that Eqn. (2.25) is a measure of the *discrete* RMS gain between the *discrete* inputs and outputs of interest. Often the designer is interested in calculating the maximum RMS gain between a continuous input and output of a sampled-data system. A good estimate of the RMS gain in this case can be found by sampling the continuous input and output of interest at a fast rate. The result is a multirate system - the input and output of interest are sampled/updated at a fast rate while the other inputs and outputs are sampled at the rate appropriate for connection to the multirate compensator. (This is also useful for determining the inter-sample behavior of a sampled-data system.) The maximum RMS gain can then be calculated using the ETIS of this new system.

### 2.5.4. Steady-State Covariance

A common measure of performance is the steady-state covariance of select outputs in response to a disturbance input. In a multirate system the "steady-state" covariance values are periodically time-varying. Fortunately, the periodic "steady-state" covariance values at each sample/update time are straightforward to calculate using the ETIS.

It is easy to show that

$$E\{y_E y_E^T\} = \begin{bmatrix} E\{y(m,0)y(m,0)^T\} \\ E\{y(m,1)y(m,0)^T\} \\ \vdots \\ E\{y(m,N-1)y(m,0)^T\} \end{bmatrix}$$

$$\begin{bmatrix} E\{y(m,0)y(m,1)^T\} & \cdots & E\{y(m,0)y(m,N-1)^T\} \\ E\{y(m,1)y(m,1)^T\} & & E\{y(m,1)y(m,N-1)^T\} \\ \vdots & \ddots & \vdots \\ E\{y(m,N-1)y(m,1)^T\} & \cdots & E\{y(m,N-1)y(m,N-1)^T\} \end{bmatrix} \tag{2.26}$$

The diagonal block elements of Eqn. (2.26) contain the steady-state covariance values at each sample/update time of the corresponding multirate system. Therefore, the steady-state covariance values can be found by calculating the ETIS of the multirate system and computing the steady-state covariance values of the ETIS using the discrete Lyapunov equation. Refer to [Kwakernaak & Sivan 1972]. Algorithms for calculating discrete covariance values are widely available (e.g., in Matlab and in $\text{Matrix}_X$).

### 2.5.5. Time Domain Simulations

Time domain simulations are straightforward to compute using the ETIS and Eqn. (2.7). As noted in Section 2.5.3, inter-sample behavior can be obtained by sampling the continuous inputs and outputs at an arbitrarily fast rate. Documentation for the M-File **mrsim**, which generates a time domain simulation of a multirate sampled-data system using the ETIS is provided in Ref. 43 (NASA TM 2002-212129).

## 2.6. SUMMARY

The tools presented in this section form the foundation of our multirate design methodology, and provide a unified approach to multirate modeling, synthesis and analysis. Using these tools one can model a complex

multirate compensator, determine the optimum values of that compensator's processor gains, and analyze its robustness and performance. In many cases the multirate systems modeling and analysis can be performed using commercially available software in conjunction with the ETIS. For those tools specific to multirate systems, including multirate compensator synthesis, documentation for custom software has been provided in Ref. 43 (NASA TM 2002-212129).

Blank

# 3. APPLICATION OF THE MULTIRATE DESIGN METHODOLOGY TO THE DESIGN OF A FLUTTER SUPPRESSION SYSTEM FOR THE BACT WING

## 3.1. INTRODUCTION

To demonstrate some of the advantages of multirate control and the capabilities of our design methodology, we designed several flutter suppression systems for NASA's BACT wing using the methodology in Section 2. A summary of our designs is presented in the following paragraphs. In Section 3.2 we describe the model wing and its open-loop characteristics. In Section 3.3 we discuss our design goals and constraints. In Section 3.4 we discuss our design approach and the details of the design process. In Section 3.5 we present our flutter suppression system design results. Finally, we end the chapter with some concluding remarks in Section 3.6.

## 3.2. THE MODEL WING AND ITS OPEN-LOOP DYNAMICS

### 3.2.1. Model Wing Description

The BACT wing was developed by NASA Langley for the Benchmark Models Program. It consists of a rigid airfoil mounted on a flexible base. The base, called the *Pitch and Plunge Apparatus* (PAPA), provides the two degrees of freedom needed to model classical wing flutter. Our designs used the single control surface (CS) located on the trailing edge of the airfoil and two accelerometers, one near the trailing edge (TE) of the airfoil and one near the leading edge (LE). A diagram of the BACT wing is shown in Fig. 3.1. A detailed description of the BACT wing can be found in [Durham, Keller, Bennett & Wieseman 1991] and [Bennett, Eckstrom, Rivera, Dansberry, Farmer & Durham 1991].

The flutter suppression system was designed using a $16^{th}$ order linear state model of the BACT wing developed by NASA Langley's Structural Dynamics Division. This model consists of 4 rigid body states corresponding to the pitch and plunge modes, 6 unsteady aerodynamic states, a second order actuator model, a second order Dryden filter, and two first order anti-aliasing filters. A block diagram of the mathematical model is shown in Fig. 3.2 on the following page.

We were provided with 24 different mathematical models of the wing. These models describe the motion of the wing in freon at 24 different operating points. The operating points include dynamic pressures above and below the critical flutter pressure at three different mach numbers. See Table 3.1 on the following page for a summary of the operating points.

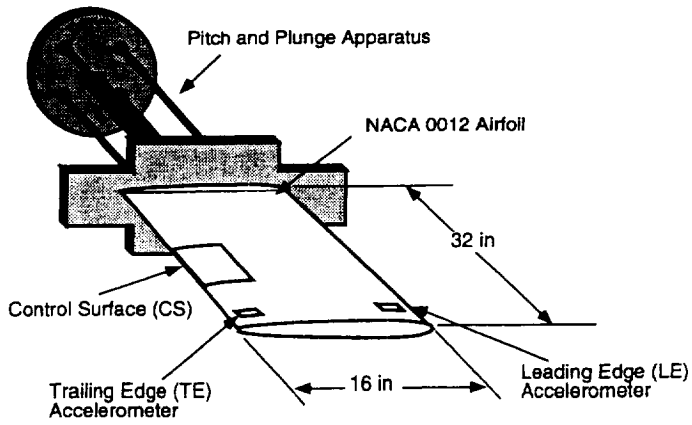


Figure 3.1. BACT wing

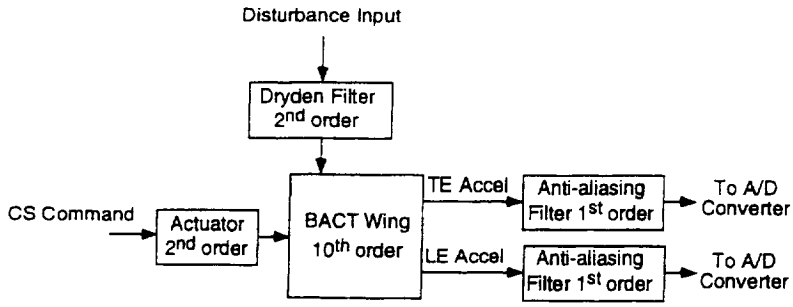


Figure 3.2. Block diagram of BACT wing

Table 3.1. Operating points for BACT wing. All operating points assume Freon medium

| | Dynamic Pressure (psf) (Nominally unstable operating points are in gray) | | | | | | | |
|---|---|---|---|---|---|---|---|---|
| Mach 0.50 | 75 | 100 | 122 | 132 | 150 | 175 | 200 | 225 |
| Mach 0.70 | 75 | 100 | 125 | 136 | 146 | 175 | 200 | 225 |
| Mach 0.78 | 75 | 100 | 125 | 141 | 151 | 175 | 200 | 225 |

### 3.2.2. Open-Loop Dynamics

The response of the open-loop BACT wing model at each operating point is characterized by two dominant modes - the pitch and plunge modes. The poles associated with pitch and plunge at mach 0.5 and 75 psf are indicated on Figs 3.3-3.4. As the dynamic pressure increases, one pair of these dominant poles moves towards the right half plane and eventually crosses the imaginary axis at the flutter stability boundary. Figures 3.5-3.6 show the migration of these dominant modes as dynamic pressure increases. The locations of the open-loop poles not shown in the figures remain relatively constant.

The dominant pitch and plunge modes are observable at all operating points with either the TE or the LE accelerometer outputs and are controllable at all operating points using the CS command input. The zeros of the CS command to TE accelerometer and the CS command to LE accelerometer transfer functions are shown in Figs. 3.3-3.4 for an operating point of mach 0.5 and 75 psf. As dynamic pressure increases, the non-minimum phase zeros associated with the TE accelerometer migrate into the left half plane. The minimum phase zeros that are associated with the LE accelerometer and located near the dominant poles migrate into the right half plane. See Figures 3.5-3.6.

At low dynamic pressures the transfer functions from CS command input to both the TE and LE accelerometer outputs are non-minimum phase. Non-minimum phase systems are typically more difficult to control than minimum phase systems. An alternative output is one which measures the difference between the two accelerometers. This new output is essentially pitch acceleration. The CS command to pitch acceleration transfer function is *minimum* phase for all operating points. Figure 3.7 shows the locations of the zeros near the pitch and plunge modes as dynamic pressure increases. It turns out that the BACT wing is fairly easy to control using this new output. The problem is that the pitch acceleration output is artificially created and assumes perfect measurement of TE and LE accelerations. In reality there is some uncertainty in the TE and LE acceleration measurements that must be accounted for in any design. Therefore we did not use the pitch acceleration output directly in our designs. We did, however, use the pitch acceleration output to determine an initial stabilizing compensator for the synthesis algorithm. This is discussed further in Section 3.4.3

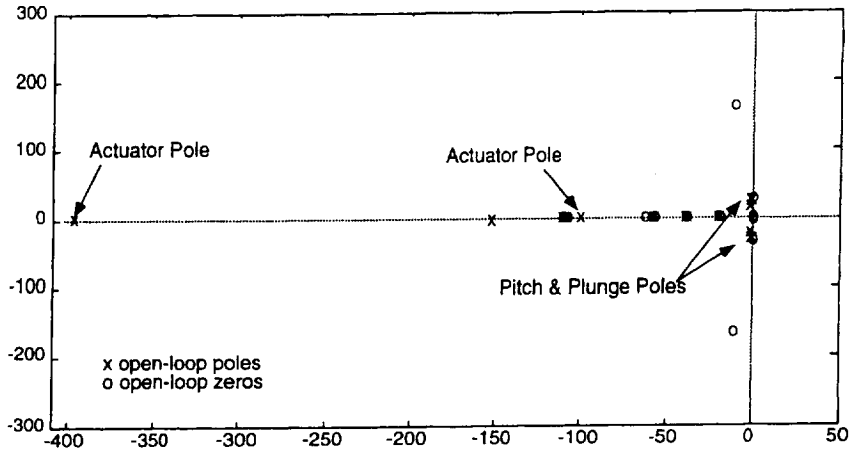


Figure 3.3. Pole/Zero map for open-loop BACT wing at mach 0.50, 75 psf for CS command to TE Accel.

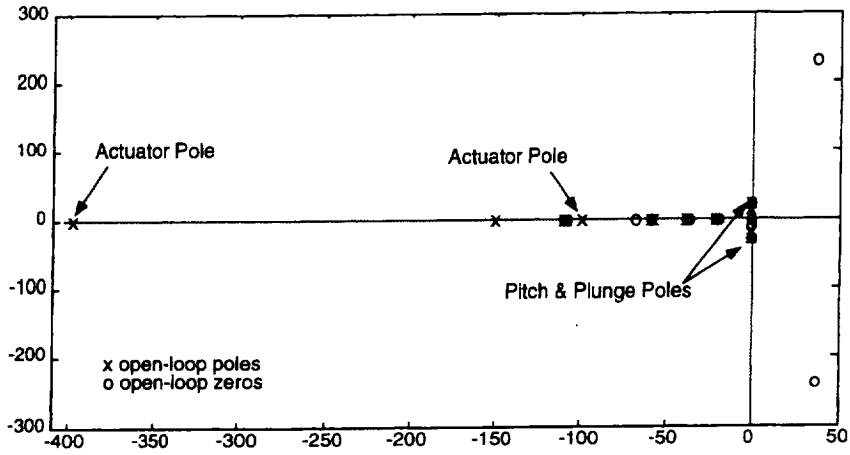


Figure 3.4. Pole/Zero map for open-loop BACT wing at mach 0.50, 75 psf for CS command to LE Accel.

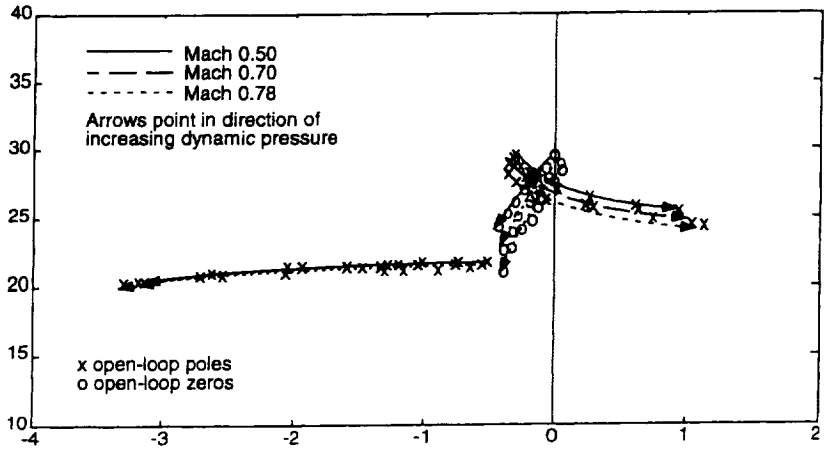


Figure 3.5. Migration of open-loop poles and zeros for CS command to TE Accel.

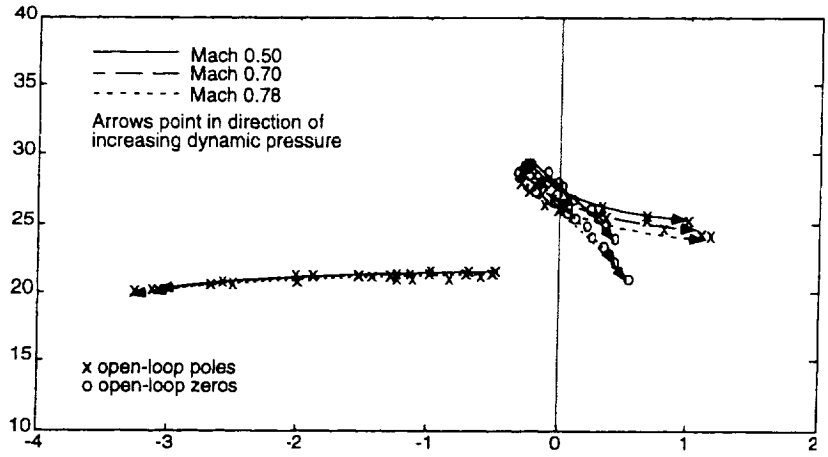


Figure 3.6. Migration of open-loop poles and zeros for CS command to LE Accel.

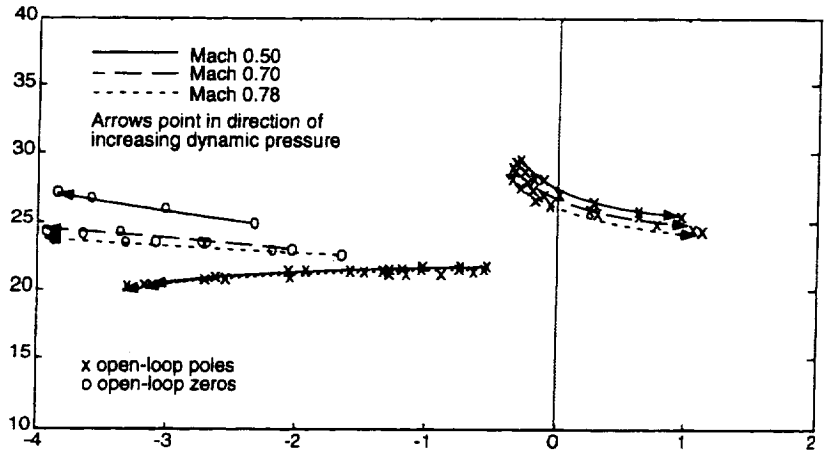


Figure 3.7. Migration of open-loop pole and zeros for CS command to TE-LE Accel.

## 3.3. DESIGN GOALS AND CONSTRAINTS

The goal of the design was to synthesize a multirate flutter suppression system which stabilizes the BACT wing at all 24 operating points. In addition to stability, NASA Langley specified the following constraints.

*Control Activity Constraint*: For unity RMS white noise input disturbance (1 in/sec RMS), the steady-state covariance of the CS deflection must not exceed 0.0625 $deg^2$ (0.25 deg RMS), and the CS deflection rate must not exceed 65 $deg^2/sec^2$ (8.0 deg/sec RMS).

*Sampling Rate Restrictions*: The minimum sampling period is 0.005 seconds. For multirate sampling all sampling periods must be multiples of 0.005 sec.

*Computational Delay*: All compensators must be designed with a minimum 0.005 second computational delay.

*Robustness Constraints*: The gain and phase margins at the compensator inputs and output must be ±6db and ±45°. At the compensator input, which has two sensors, we use the generalized gain and phase margins based on the singular value. The specified gain and phase margins correspond to a minimum value of 0.75 for the maximum singular value of a multiplicative uncertainty at the compensator inputs (see [Mukhopdhyay & Newsom 1984]).

## 3.4. FLUTTER SUPPRESSION SYSTEM DESIGN

We used the methodology discussed in Section 2 to design the flutter suppression system. The specific steps for this design were:

1) Select an LQR cost function such that the BACT wing in feedback with the LQ regulator satisfies the criterion specified by NASA
2) Choose an appropriate multirate compensator structure and sampling schedule based on this LQR design
3) Find a set of processor gains so that the compensator stabilizes the BACT wing
4) Synthesize a multirate compensator which minimizes the LQR cost function of step (1) at a few select operating points using the algorithm discussed in Section 2.4
5) Check the performance and robustness of the closed-loop system
6) Iterate on items (1)-(5) as required

We elaborate on the details of each step in the following paragraphs.

### 3.4.1. Selecting the Cost Function Weights

The multirate synthesis algorithm finds optimum values of the compensator's digital processor gains by minimizing a quadratic cost function with respect to those gains. This optimization can be performed for multiple plant conditions simultaneously. We used the multiple plant capabilities of the algorithm to help ensure that the compensator stabilizes the wing at all 24 operating points. Instead of using all 24 operating points for the optimization we used six representative ones. The six include the operating points at the extremes of mach number and dynamic pressure, and two operating points midway between the extremes. These operating points are listed in Table 3.2 on the following page. For the fault tolerant design discussed in Section 3.4.2.4 we included four additional operating points at mach 0.50. These operating points are grayed in Table 3.2.

For each operating point we selected a unique set of weights for the synthesis algorithm's cost function. The weights were based on a continuous LQR design which weighted the pitch and plunge modes, and the CS command input of the BACT wing. The cost function has the form

$$J = \lim_{t\to\infty} E\left\{\mathbf{x}(t)^{\mathrm{T}} Q_1\, \mathbf{x}(t) + u(t)^{\mathrm{T}} Q_2\, u(t)\right\} \tag{3.1}$$

where $x = \{x_1 \;\; x_2 \;\; x_3 \;\; x_4\}^{\mathrm{T}}$ and the $x_i$ are the four states associated with the pitch and plunge mode in a modalized version of the BACT wing model. States $x_1$ and $x_2$ correspond to the complex conjugate poles which migrate to the left as dynamic pressure increases, see Fig. 3.5. States $x_3$ and $x_4$ correspond to the complex conjugate poles which migrate to the right as dynamic pressure increases, see Fig. 3.5. The latter set of poles cause instability in the BACT wing at high dynamic pressures. The variable $u$ is the CS command signal.

For each operating point, the weights, $Q_1$ and $Q_2$, were chosen so that the closed-loop damping of the pitch and plunge modes was greater than 0.07, and the RMS control constraints specified by NASA were satisfied. For comparison, the damping in the open-loop BACT wing at the stable dynamic pressure of 75 psf is

approximately 0.025. The weights for each operating point were scaled to obtain a unity LQR cost for a 6 inch/sec RMS white noise disturbance input.

Table 3.2. Cost function weights. Grayed operating points used only for fault tolerant design.

| Operating Point | | State Weight ($Q_1$) | Control Weight ($Q_2$) |
|---|---|---|---|
| Mach 0.50 | 75 psf | diag[$1.2\text{x}10^{-2}$ $1.2\text{x}10^{-2}$ 12 12] | 610 |
| Mach 0.50 | 132 psf | diag[$5.0\text{x}10^{-3}$ $5.0\text{x}10^{-3}$ 3.5 3.5] | 500 |
| Mach 0.50 | 150 psf | diag[$5.0\text{x}10^{-3}$ $5.0\text{x}10^{-3}$ 2.5 2.5] | 750 |
| Mach 0.50 | 175 psf | diag[$4.5\text{x}10^{-3}$ $4.5\text{x}10^{-3}$ 1.4 1.4] | 900 |
| Mach 0.50 | 200 psf | diag[$5.8\text{x}10^{-3}$ $5.8\text{x}10^{-3}$ 0.58 0.58] | 1754 |
| Mach 0.50 | 225 psf | diag[$9.6\text{x}10^{-4}$ $9.6\text{x}10^{-4}$ $9.6\text{x}10^{-2}$ $9.6\text{x}10^{-2}$] | 4800 |
| Mach 0.70 | 125 psf | diag[$1.3\text{x}10^{-2}$ $1.3\text{x}10^{-2}$ 6.4 6.4] | 3900 |
| Mach 0.70 | 175 psf | diag[$1.9\text{x}10^{-3}$ $1.9\text{x}10^{-3}$ 0.56 0.56] | 5600 |
| Mach 0.78 | 75 psf | diag[$8.8\text{x}10^{-2}$ $8.8\text{x}10^{-2}$ 44 44] | 8800 |
| Mach 0.78 | 225 psf | diag[$3.3\text{x}10^{-4}$ $3.3\text{x}10^{-4}$ $1.6\text{x}10^{-2}$ $1.6\text{x}10^{-2}$] | 26000 |

### 3.4.2. Selecting the Compensator Structure and Sample Rate

Traditionally, the design of a multirate compensator structure begins with a successive loop closures structure and then incorporates cross feed between the loops as necessary. As discussed in Section 2.4.1, multirate successive loop closures is best applied to problems in which the closed-loop system dynamics can be separated into some fast dynamics and some slow dynamics. The BACT wing however does not exhibit those closed-loop characteristics. Closed-loop bode plots, from control input to accelerometer outputs of the BACT wing in feedback with a LQ Regulator, are shown in Fig. 3.8. The LQ Regulator was designed using the cost function weights for the mach 0.50 75 psf operating point specified in Table 3.2. Therefore the bode plot is representative of the closed-loop dynamics we are trying to achieve with the flutter suppression system. Notice that the closed-loop dynamics have only one peak - that associated with the pitch and plunge modes - and do not exhibit the fast and slow dynamics traditionally associated with successive loop closures. Consequently, a traditional multirate successive loop closure structure is not directly applicable to this problem.

Instead of basing our multirate compensator structure on the closed-loop dynamics of the system, we selected compensator structures which used different sampling schedules to reduce either the number of computations or the hardware required to implement the compensator. We designed four compensators: a single-rate (SR); a multirate successive loop closures type (MRSLC); a multirate with multiplexed inputs (MRMI); and a single-rate fault tolerant (SRFT). All of these compensators are second order except the fault tolerant design which is fourth order.

#### *3.4.2.1. Single-Rate (SR)*

The single-rate compensator was designed for comparison with the other compensators. A block diagram of this compensator is shown in Fig. 3.9. The sample/update rate for this compensator is 50 Hz. This rate is approximately 10 times the frequency of the dominant pitch and plunge modes. The compensator includes a 0.02 second computational delay, which satisfies NASA's computational delay requirement. This was achieved by constraining the compensator's direct feedthrough term to be zero.

The state space structure of the compensator is

$$\begin{Bmatrix} \bar{z}_1(m,n+1) \\ \bar{z}_2(m,n+1) \end{Bmatrix} = \begin{bmatrix} 0 & 1 \\ a_1 & a_2 \end{bmatrix} \begin{Bmatrix} \bar{z}_1(m,n) \\ \bar{z}_2(m,n) \end{Bmatrix} + \begin{bmatrix} 0 & b_1 \\ 1 & b_2 \end{bmatrix} \begin{Bmatrix} \text{TE Accel}(m,n) \\ \text{LE Accel}(m,n) \end{Bmatrix} \tag{3.2a}$$

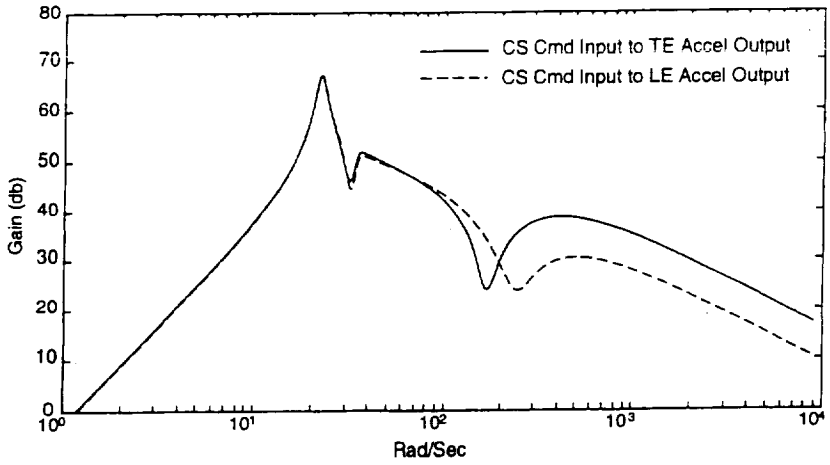


Figure 3.8. Bode plot of closed-loop BACT wing with LQ regulator at mach 0.5 75 psf

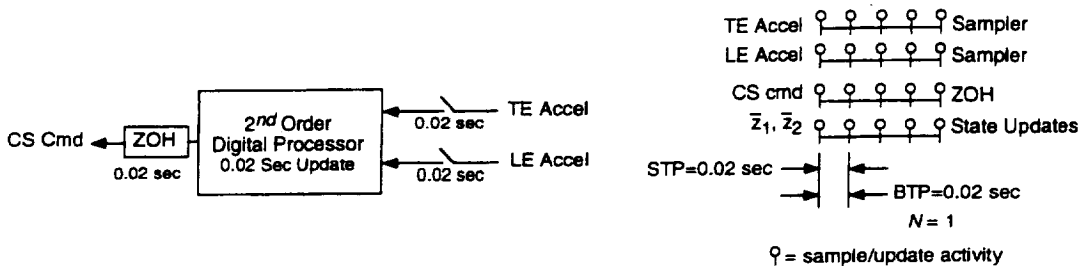


Figure 3.9. Block diagram and corresponding sampling schedule for the SR compensator

$$\text{CS Cmd}(m,n) = \begin{bmatrix} c_1 & c_2 \end{bmatrix} \begin{Bmatrix} \bar{z}_1(m,n) \\ \bar{z}_2(m,n) \end{Bmatrix} \tag{3.2b}$$

where $\bar{z}_1$ and $\bar{z}_2$ are the digital processor states; TE Accel and LE Accel are the acceleration inputs from the A/D converters; and CS Cmd is the command output to the zero-order-hold. $a_i$, $b_i$, and $c_i$ are the free gains (matrix elements) which were optimized. The other gains were constrained to the values shown. The structure in Eqn. (3.2) is a minimum realization of the second order compensator. See [Berg, Mason & Yang 1991] for a discussion of minimum realizations. The sampling schedule for Eqn. (3.2) is shown in Fig. 3.9.

*3.4.2.2. Multirate Successive Loop Closures (MRSLC)*

The MRSLC compensator was designed to reduce the total number of multiplications per unit time performed by the compensator's digital processor. The compensator is comprised of two first order loops. Both loops have two inputs, TE and LE acceleration, and one output, CS command. One of the loops is sampled/updated at 50 Hz, the same as the single-rate design, and the other is sampled/updated four times slower at 12.5 Hz. Just as in the single-rate design, the direct feedthrough terms were constrained to be zero, resulting in a 0.02 second computational delay.

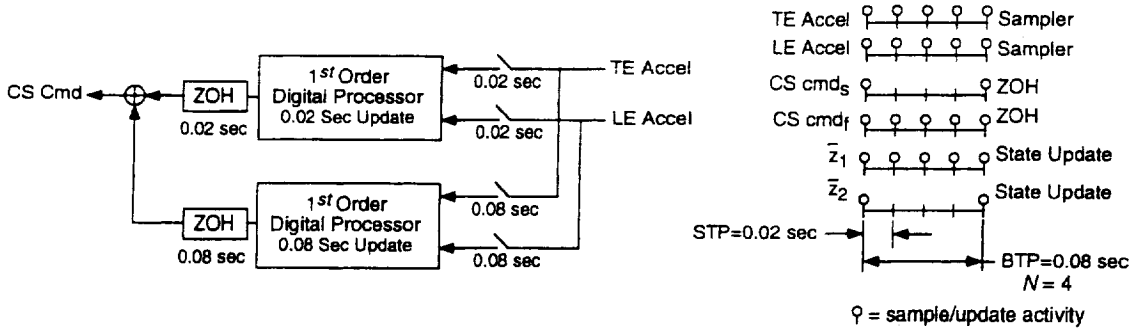


Figure 3.10. Block diagram and corresponding sampling schedule for the MRSLC compensator

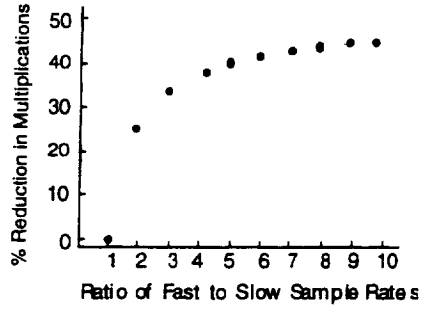


Figure 3.11. Computational savings with the MRSLC design

The net result of this two loop configuration is a compensator structure just like the single-rate design except that the digital processor needs to update one of the digital processor states only every fourth sample/update period. A block diagram of this compensator along with a diagram of its sampling schedule is shown in Fig. 3.10. Note that this diagram only illustrates the structure of the compensator - it is not a schematic of how the compensator would be implemented. When actually implemented, this compensator will use the same number of D/A and A/D converters as the SR compensator, but will require 37% fewer real-time multiplications per unit time.

The choice of sample/update rates for the slow loop was arbitrary within the constraints of the GMCLS. Our goal was simply to reduce the number of multiplications required by the compensator without significantly degrading its performance. The 12.5 Hz sample/update rate was chosen because it is a good compromise between the total number of multiplications saved by utilizing this multirate structure and the ratio of the fast to slow sampling rates. Figure 3.11 shows the percent reduction in the number of multiplication by using the MRSLC design over the SR design. There is a decreasing return in computational savings as the ratio of the fast to slow sampling rate increases. In the limit, the compensator degenerates to a first order compensator with a reduction in multiplications of 50%. Based on Fig. 3.11 we chose a sampling rate ratio of 4.

The state space structure of the compensator which was used for the optimization is

$$\begin{Bmatrix} \bar{z}_1(m,n+1) \\ \bar{z}_2(m,n+1) \end{Bmatrix} = \begin{bmatrix} a_f & 0 \\ 0 & a_s \end{bmatrix} \begin{Bmatrix} \bar{z}_1(m,n) \\ \bar{z}_2(m,n) \end{Bmatrix} + \begin{bmatrix} 1 & b_1 \\ 1 & b_2 \end{bmatrix} \begin{Bmatrix} \text{TE Accel}(m,n) \\ \text{LE Accel}(m,n) \end{Bmatrix} \tag{3.3a}$$

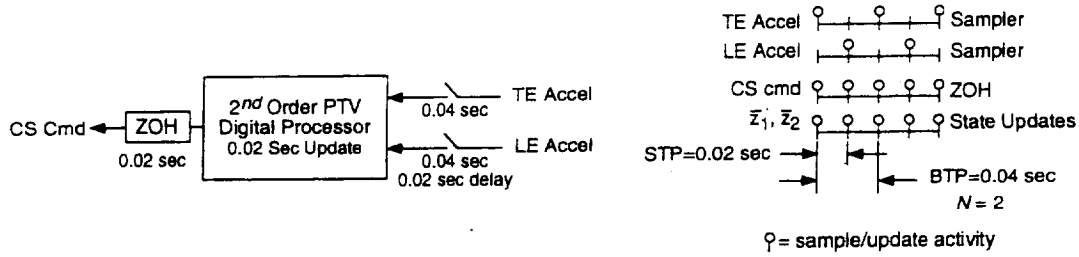


Figure 3.12. Block diagram and corresponding sampling schedule for the MRMI compensator

$$\begin{Bmatrix} \text{CS Cmd}_f(m,n) \\ \text{CS Cmd}_s(m,n) \end{Bmatrix} = \begin{bmatrix} c_f & 0 \\ 0 & c_s \end{bmatrix} \begin{Bmatrix} \bar{z}_1(m,n) \\ \bar{z}_2(m,n) \end{Bmatrix} \tag{3.3b}$$

$$\text{CS Cmd}(m,n) = \text{CS Cmd}_f(m,n) + \text{CS Cmd}_s(m,n) \tag{3.3c}$$

where $\bar{z}_1$ and $\bar{z}_2$ are the digital processor states; TE Accel and LE Accel are the acceleration inputs from the A/D converters; and CS Cmd is the command output to the zero-order-hold. $a_i$, $b_i$, and $c_i$ are the free gains which were optimized. The other gains were constrained to the values shown. The structure in Eqn. (3.3) corresponds to the successive loop closures structure of Fig. 3.10. The intermediate outputs CS $\text{Cmp}_f$ and CS $\text{Cmp}_s$ were added to ensure that Eqn. (3.3) corresponded to Fig. 3.10.

*3.4.2.3. Multirate with Multiplexed Inputs (MRMI)*

The multirate compensator with multiplex inputs was designed to reduce the number of A/D converters required to implement the SR design. In this design, the compensator state and output updates occur at 50 Hz. The outputs of the TE and LE accelerometers are sampled at 25 Hz with a 0.02 second delay between the sampling of the TE accelerometer output and the LE accelerometer output. Thus, the MRMI requires only one A/D converter to sample both accelerometer outputs because it can be multiplexed between the two signals. In addition, the digital processor gains for the MRMI compensator are periodically time-varying. One set of gains is used when the TE accelerometer output is sampled and another set is used when the LE accelerometer output is sampled. Just as in the single-rate design, the direct feedthrough terms were constrained to be zero, resulting in a 0.02 second computational delay. This compensator requires the same number of multiplications per unit time as the SR design but it uses only one D/A converter. Figure 3.12 shows a block diagram of the MRMI compensator.

The state space structure of the MRMI compensator is

$$\begin{Bmatrix} \bar{z}_1(m,n+1) \\ \bar{z}_2(m,n+1) \end{Bmatrix} = \begin{bmatrix} 0 & 1 \\ a_1(n) & a_2(n) \end{bmatrix} \begin{Bmatrix} \bar{z}_1(m,n) \\ \bar{z}_2(m,n) \end{Bmatrix} + \begin{bmatrix} 0 & b_1(n) \\ 1 & b_2(n) \end{bmatrix} \begin{Bmatrix} \text{TE Accel}(m,n) \\ \text{LE Accel}(m,n) \end{Bmatrix} \tag{3.4a}$$

$$\text{CS Cmd}(m,n) = \begin{bmatrix} c_1(n) & c_2(n) \end{bmatrix} \begin{Bmatrix} \bar{z}_1(m,n) \\ \bar{z}_2(m,n) \end{Bmatrix} \tag{3.4b}$$

where $\bar{z}_1$ and $\bar{z}_2$ are the digital processor states; TE Accel and LE Accel are the acceleration inputs from the A/D converters; and CS Cmd is the command output to the zero-order-hold. $a_i(n)$, $b_i(n)$, and $c_i(n)$ are the free gains which were optimized. These gains are functions of $n$ because they are periodically time-varying, e.g. $a_i(n) = a_i(n+2)$ The other gains were constrained to the values shown. The sampling schedule for Eqn. (3.4) is shown in Fig. 3.12.

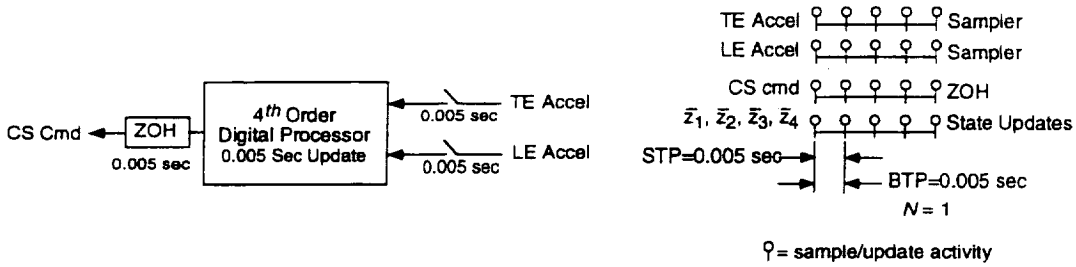


Figure 3.13. Block diagram and corresponding sampling schedule for the SRFT compensator

*3.4.2.4. Single-Rate Fault Tolerant (SRFT)*

The single-rate fault tolerant compensator was designed to highlight the multiple plant capability of our synthesis algorithm. This compensator is fourth order with a sample/update rate of 200 Hz and a 0.005 second computational delay. A block diagram of the compensator and its corresponding sampling schedule are shown in Fig. 3.13. The state space representations of the SRFT compensator is similar to the $2^{nd}$ order single-rate compensator with the exception that the digital processor is fourth order.

The SRFT compensator is fault tolerant in the sense that it stabilizes all the plant conditions even with one of the accelerometers disconnected. To achieve fault tolerance for all 24 plant conditions, we optimized the compensator for 22 simultaneous plant conditions - as opposed to just six for the preceding designs. These include the six operating points used in the previous designs evaluated at three cases each: 1) both TE and LE sensors active; 2) only the TE sensor active; and 3) only the LE sensor active. In addition to those 18, we added four more operating points at mach 0.50 evaluated for the case where only the LE sensor is active. These operating points are grayed in Table 3.2.

### 3.4.3. Designing a Stabilizing Compensator

We used the synthesis algorithm presented in Section 2.4 to optimize the gains of the four compensators discussed in Section 3.4.2. The algorithm requires an initial guess for the compensator's digital processor gains for which the closed-loop system, the BACT wing and compensator, is stable. The difficulty in finding these gains is that the closed-loop system must be stable at all operating points used in the optimization.

To get a stabilizing guess for the wing at all operating points we used a boot-strapping technique. First we found values of the processor gains which stabilized the BACT wing at *one* operating point. Then we optimized the gains for the wing at that *one* operating point using large values for the plant disturbance noise and sensor noise intensities. The large value of noise intensities introduced uncertainty into the plant. Consequently, the resulting compensator was more robust than a compensator optimized for a plant with no noise. This new set of processor gains always stabilized the wing at the original operating point plus at least one other operating point. We then used the new processor gains as the initial guess to the problem with the wing at two (or more) operating points. The procedure was continued until the compensator stabilized the plant at all the operating points and the problem could be solved using realistic noise intensities.

Before beginning the bootstrapping procedure we needed to find a set of processor gains which stabilized the closed-loop system for at least one operating point. This was straightforward for the SR and MRSLC compensators. We designed a first order single-rate compensator with pitch acceleration input, CS command output and a sampling rate of 50 Hz. Recall from Section 3.2.2 that pitch acceleration is essentially the difference in the TE and LE accelerations. The pole location and gain value of this compensator were found using root locus. The initial stabilizing guess for the SR design consisted of this first order compensator in parallel with an arbitrary first order compensator that had an input/output gain of zero. For the MRSLC system,

we used the first order compensator as an initial guess for the fast loop of the successive loop closures structure, and an arbitrary first order compensator, with an input/output gain of zero, for the slow loop.

An initial guess for the MRMI processor gains was more difficult to find than for the SR and MRSLC compensators. Due to its complex sampling schedule we could not design an initial guess by traditional methods. Instead, we designed a compensator with the multiplexed structure but with very small gains. Then we used the bootstrapping technique, beginning with the BACT wing operating at a low dynamic pressure where it is open-loop stable. Since the compensator gains were very small, they did not destabilize the wing and could be used as an initial guess. The bootstrapping process for this compensator took several iterations, verses one or two for the other compensators, because we began with such a poor initial guess.

To obtain an initial guess for the SRFT processor gains we began by designing two $2^{nd}$ order compensators. One stabilized the plant when the LE sensor was disconnected, the other stabilized the plant when the TE was disconnected. We then combined these two compensators into a single $4^{th}$ order design and adjusted their gains until the new fourth order compensator stabilized the plant when both sensors were active or when only one or the other was active. Finally this design was used in the bootstrapping procedure discussed earlier to obtain a single fourth order compensator which stabilized the wing at all operating points.

### 3.4.4. Optimizing the Digital Processor Gains

We optimized the digital processor gains of the three compensators with the algorithm discussed in Section 2.4. The optimization used the following parameters:

| | |
|---|---|
| Plant Conditions: | Six simultaneous operating points for the second order designs; 22 simultaneous operating points for the fourth order design. See Table 3.2 and Section 3.4.2.4 |
| Cost Function Weights: | The second order designs used the cost function weights listed in Table 3.2. The fourth order design used the weights in Table 3.2 for cases where both the TE and LE sensors were active, and one-tenth those values for cases where either sensor was inactive |
| Process Noise PSD value: | 36 $in^2/sec^2$ - this is the intensity of the white noise input to the Dryden filter and was specified by NASA |
| Sensor Noise PSD value: | 0 $rad^2/sec^4$ for initial designs, 240 $rad^2/sec^4$ for final designs. This is discrete sensor noise for the TE and LE acceleration measurements |
| Initial Stabilizing Gains: | Obtained using root locus and boot strapping, see Section 3.4.3 |
| Compensator Structure: | See equations (3.2)-(3.4) |
| Sampling Schedule: | See Figures 3.9, 3.10, 3.12 and 3.13. |
| Gain Constraints: | In all designs the direct feed through terms were constrained to be zero. Additional gain constraints for each compensator are specified in Section 3.4.2. |

The M-Files which define the above input parameters for the synthesis software presented in Ref. 43 are documented in Appendix B

### 3.4.5. Design Iteration Based on Performance and Robustness Analysis

After synthesizing the multirate compensators we evaluated their performance and robustness using the methods discussed in Section 2.5. One of the robustness measures was the maximum singular value of the minimum destabilizing multiplicative uncertainty at the compensator inputs (a structured singular value). When we synthesized the compensators using a sensor noise covariance intensity of zero, the size of the destabilizing

gain was unacceptably small - less than 0.20 for the BACT wing at some operating points. NASA had specified a value of 0.75. To improve the robustness at the compensator input we increased the sensor noise intensity to 240 $rad^2/sec^4$ and re-optimized the processor gains. This procedure was motivated by the Loop Transfer Recover technique for LQG systems described in [Doyle & Stein 1981]. The results of increasing the sensor noise are discussed in the following Section.

### 3.5. DESIGN RESULTS

We designed four compensators using the approach discussed in the previous sections. For review, the four are the:

1) Single-Rate $2^{nd}$ Order (SR)
2) Multirate $2^{nd}$ Order Successive Loop Closures (MRSLC)
3) Multirate $2^{nd}$ Order Multiplexed Input (MRMI)
4) Single-Rate Fault Tolerant (SRFT)

The structure of each of these compensators was discussed in Section 3.4.2. Optimum values for the digital processor gains are given in Appendix A.

We looked at five performance and robustness measures:

1) Cost function value
2) Gust pulse response
3) Maximum RMS gain from disturbance to the control surface deflection and deflection rate
4) Gain and phase margins at the compensator output
5) The maximum singular value of the minimum destabilizing multiplicative uncertainty at the compensator input

Results are presented for three operating points, mach 0.50 132 psf, mach 0.70 146 psf, and mach 0.78 151 psf. Each of these operating points is 5 psf above the critical flutter dynamic pressure for the corresponding mach number, and so the BACT wing is nominally unstable at each of these operating points. It is important to note that none of these operating points were used for the compensator optimization. Therefore the compensators were not tuned to these particular operating points. In general, the performance and robustness of the compensators at these three operating points is indicative of their performance at the remaining 21 operating points.

#### 3.5.1. Cost Function Value

One measure of the overall steady-state performance of a compensator is the value of the cost function in Eqn. (3.1) at the optimum value of the digital processor gains. (A value for the cost function is returned by our synthesis algorithm at the completion of the optimization.) For our $2^{nd}$ order designs, a "perfect" compensator would have a cost function value of 6, assuming no sensor noise. The "perfect" fault tolerant design would have a cost of 7.6 since it optimizes a different cost function. By "perfect" compensators we mean continuous LQR designs with gain scheduling, i.e., they use a different set of feedback gains at every operating point. We expect the costs associated with our compensators to be higher since they used discrete sampling, did not use gain scheduling, and had fictitious sensor noise.

It is more realistic to compare the cost of our compensators to that of a discrete LQG design with fictitious sensor noise and gain scheduling. This comparison eliminates some of the differences due to sampling and fictitious sensor noise. The cost associated with the discrete LQG compensator is the lowest cost we can expect

for a given sampling rate and sensor noise level. Table 3.3 summarizes the values of the cost function for the discrete LQG and for our four designs. The costs associated with our second order compensators are almost twice that of the discrete LQG design. This is not surprising since the discrete LQG is significantly more complex - it is a $16^{th}$ order compensator with gain scheduling.

### 3.5.2. The Gust Pulse Response

The gust pulse response provides an indication of the transient response of the closed-loop system due to a disturbance input. The gust pulse response was found by simulating the response of the BACT wing in feedback with the flutter suppression system to a disturbance input pulse with an amplitude of 10 in/sec and a duration of 0.004 seconds. This simulation was performed using the M-file **mrsim** described in Attachment 4.

Figures 3.14-3.16 show the response of the BACT wing at mach 0.70 and 146 psf to the specified disturbance gust pulse. Also shown is the response of the wing with a continuous LQ regulator. The cost function weights for this LQ regulator design satisfy the same design criterion as was used to optimize the compensator's gains. (See Section 3.4.1.) We provided response plots for only one operating point. The gust pulse responses at other operating points are similar to those provided in Figs. 3.14-3.16.

For comparison we also provided a gust pulse response plot for the $2^{nd}$ order compensators synthesized without fictitious sensor noise. Recall that fictitious noise was added to the sensors in order to improve the robustness at the compensator input. Figure 3.17 shows the pitch response of the BACT wing at mach 0.70 and 146 psf due to a gust pulse disturbance. The primary effect of adding sensor noise is to decrease the damping of the pitch and plunge modes. The reduction in damping is more prevalent in the pitch response than in the plunge response.

The gust pulse response plots are shown below.

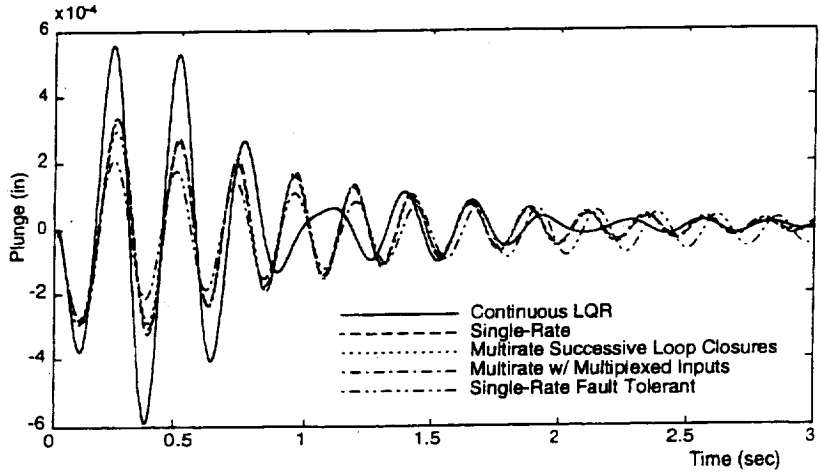


Figure 3.14. Plunge gust pulse response at mach 0.70 146 psf

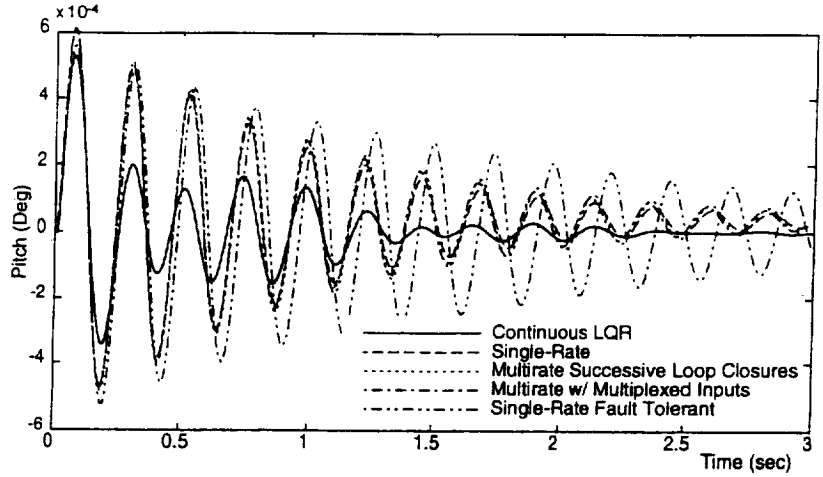


Figure 3.15. Pitch gust pulse response at mach 0.70 146 psf

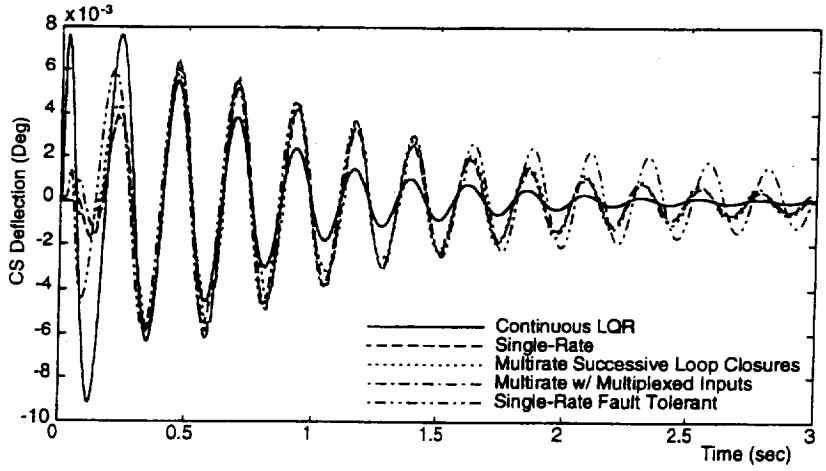


Figure 3.16. Control surface deflection gust pulse response at mach 0.70 146 psf

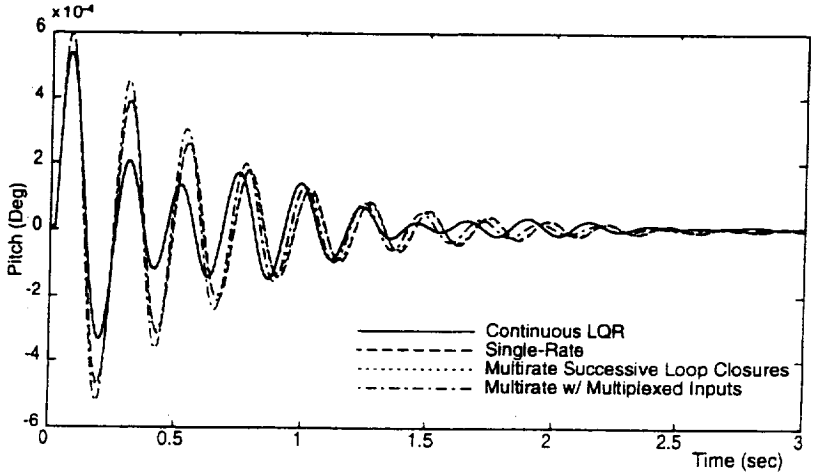


Figure 3.17. Pitch gust pulse responses at Mach 0.70 146 psf for compensator designed without fictitious sensor noise

Table 3.3 Design Results

| | Mach 0.50, 132 psf | | | | Mach 0.70, 146 psf | | | | Mach 0.78, 151 psf | | | |
|---|---|---|---|---|---|---|---|---|---|---|---|---|
| | SR | MRSLC | MRMI | SRFT | SR | MRSLC | MRMI | SRFT | SR | MRSLC | MRMI | SRFT |
| Cost Function Value [1] | 13.9[2] | 14.2[2] | 15.6[2] | 26.0[3] | | | | | | | | |
| Max RMS Gain Distr. to CS Deflect. (deg sec/in) | 0.22 | 0.22 | 0.25 | 0.22 | 0.19 | 0.19 | 0.19 | 0.13 | 0.11 | 0.11 | 0.11 | 0.11 |
| Distr. to CS Def-Rate (deg/in) | 6.5 | 6.6 | 6.9 | 6.2 | 2.4 | 2.8 | 2.6 | 3.4 | 1.5 | 1.6 | 1.5 | 2.8 |
| Gain Margin | 12 db | 14 db | 12 db | 8 db | 10 db | 12 db | 10 db | 6 db | 9 db | 11 db | 9 db | 5 db |
| Phase Margin | 41° | 45° | 38° | 21° | 45° | 48° | 40° | 18° | 43° | 48° | 40° | 15° |
| $\overline{\sigma}\begin{bmatrix} k_1 & 0 \\ 0 & k_2 \end{bmatrix}$ | 0.41 | 0.49 | 0.45 | 0.35 | 0.38 | 0.48 | 0.44 | 0.28 | 0.35 | 0.49 | 0.45 | 0.25 |
| $\overline{\sigma}\begin{bmatrix} k_1 & 0 \\ 0 & k_2 \end{bmatrix}$ w/o sensor noise | 0.25 | 0.25 | 0.35 | not calculated | 0.26 | 0.23 | 0.32 | not calculated | 0.25 | 0.21 | 0.31 | not calculated |

[1] Cost Function Value is not a function of the operating point

[2] The corresponding discrete LQG cost is 7.7

[3] The corresponding discrete LQG cost is 8.6

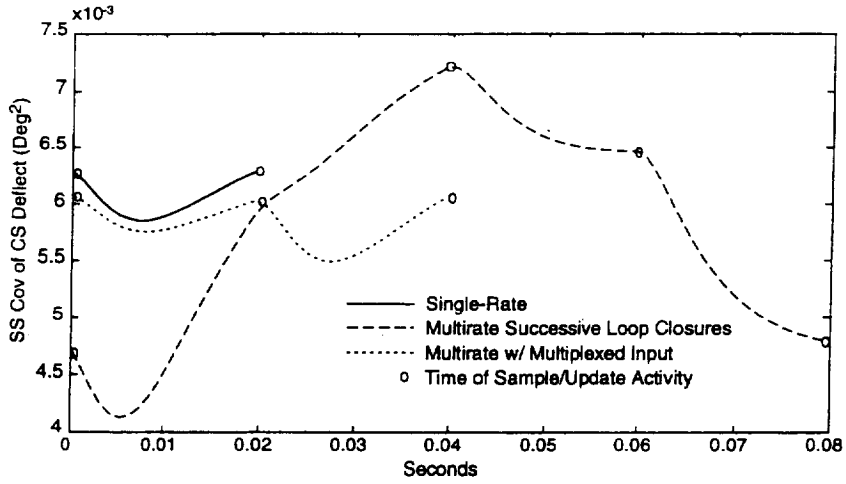


Figure 3.18. Steady-state covariance propagation at mach 0.70 146 psf with 1 in/sec RMS white noise disturbance

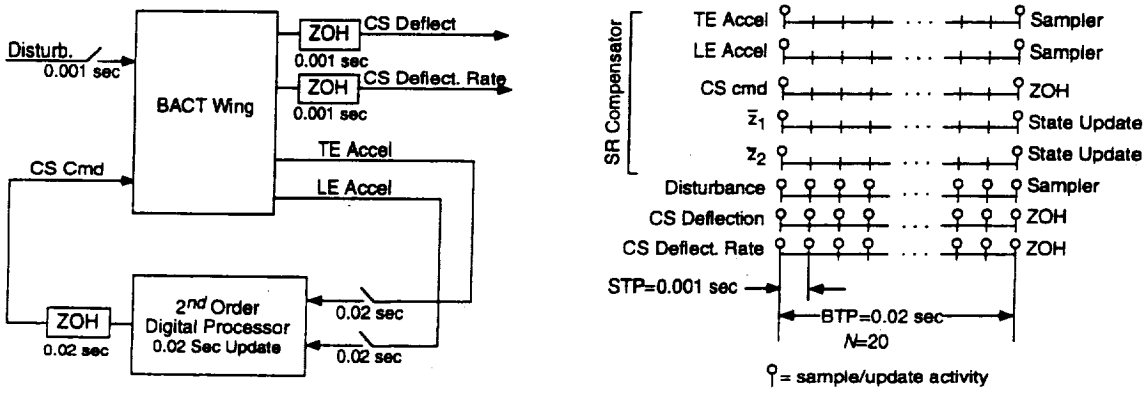


Figure 3.19. Block diagram of discrete system for calculating RMS gain and corresponding sampling schedule

### 3.5.3. RMS Gain for Control Surface Deflection and Deflection Rate

One of NASA's specifications was a limit on the steady-state covariance of the control surface deflection and deflection rate for a 1 in/sec RMS white noise disturbance. Our closed-loop system consists of a continuous plant and a discrete compensator. Therefore these steady-state covariances are periodically time-varying. In Fig. 3.18 we show the steady-state covariance propagation for the BACT wing in feedback with the three compensators at an operating point of mach 0.70 and 146 psf for a unity RMS white noise disturbance.

We calculated the values of the steady-state covariance at the sample/update times using the method described in Section 2.5.4. Between the sample/update times of the compensator, the covariances were propagated using the dynamics of the open-loop continuous BACT wing. The steady-state covariances are only shown for one BTP of the compensator - they repeat themselves during every BTP of the compensator.

One meaningful interpretation of NASA's specification would be to look at the peak steady-state covariance value taken from this covariance plot. This value, though, is an upper limit on the closed-loop gain for a white noise disturbance and is not an accurate indicator of the control activity level. A better measure of

control activity would be the maximum RMS gain calculated using Eqn. 2.25. This is an exact measure of the maximum RMS gain for *any* non-decaying input signal.

In order to apply Eqn. (2.25), which is for a discrete system, to our mixed continuous/discrete system we created a new discrete multirate system in which the continuous inputs and outputs of interest are sampled very fast (see Section 2.5.3). We chose a sampling rate for the CS deflection and deflection rate of 1000 Hz. This is more than twenty times the control surface actuator rolloff frequency. A block diagram of this new discrete-time system, with the single-rate compensator of Eqn. (3.2), is shown in Fig. 3.19 along with its sampling schedule. This new system is now *multirate* even though the compensator is *single-rate*. The ETIS for this system has a sample/update rate of 1000 Hz and an $N$ of 20.

We used this new ETIS system to calculate the maximum RMS gain of the original system between the disturbance and the CS deflection and between the disturbance and the CS deflection rate. The maximum RMS gains for the BACT wing at three operating points are summarized in Table 3.3. See also the related work of [Sivashankar & Khargonekar 1991].

### 3.5.4. Gain and Phase Margins at the Compensator Output

Gain and phase margins were calculated at the compensator output using the ETIS and a multiloop Nyquist diagram. The ETIS of the plant and compensator were computed independently and then combined in series to form an ETIS loop transfer function. Gain and phase margins were subsequently measured directly off the multiloop Nyquist plot of this function. These are traditional gain and phase margins, and assume that the gain and phase do not vary simultaneously. The details of this technique are given in Section 2.5.1, [Mason 1992], and [Mason & Berg 1992]

The gain and phase margins for the BACT wing at three operating points are presented in Table 3.3. These values are typical of the margins at all 24 operating points, although the margins tend to be better at lower dynamic pressures and slightly worse at higher dynamic pressures. A representative Nyquist diagram is shown in Fig. 3.20. This particular Nyquist plot has two encirclements of the –1 point because the open-loop plant has two unstable poles.

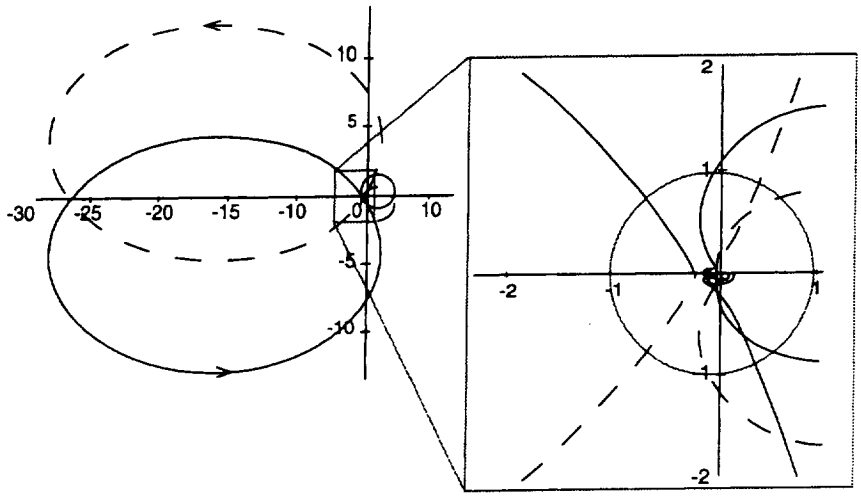


Figure 3.20. Multiloop Nyquist for BACT wing at mach 0.70 146 psf with MRMI compensator

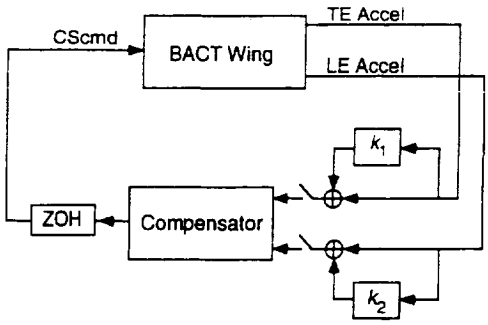


Figure 3.21. Uncertainty Model

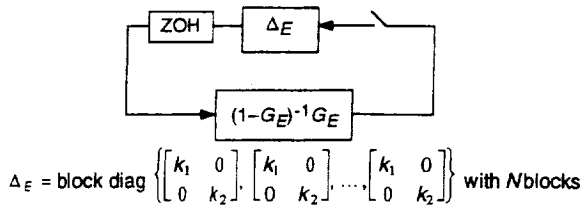


Figure 3.22 ETIS uncertainty output feedback model

### 3.5.5. Robustness at the Compensator Input

The uncertainty at the compensator input was assumed to be a multiplicative perturbation of the form shown in Fig. 3.21, where $k_1$ and $k_2$ are complex gains. We transformed this system into the output feedback form traditionally used in robustness analysis using simple block diagram algebra. However, when the compensator is multirate we must use the ETIS of the plant, compensator and uncertainty. A block diagram of this closed-loop ETIS for the multirate flutter suppression system is shown in Fig. 3.22. $G_E$ is the loop transfer function consisting of the compensator and plant ETIS transfer functions connected in series.

Now, given the system in the form shown in Fig. 3.22, we can calculate an exact value for the size of the smallest destabilizing perturbation [Doyle 1982] . First rewrite $\Delta_E$ in Fig. 3.22 as

$$\Delta_E = I_1 k_1 + I_2 k_2 \tag{3.5}$$

where $I_1$ = diag{1 0 1 0 ... 1 0} with $2N$ diagonal elements, and where $I_2$ has a similar form. Then it can be shown that

$$\bar{\sigma}(\Delta_{\min}) = \left( \sup_{\phi} \max_{\theta} \rho\left\{\left[I_1 + I_2 e^{j\theta}\right] H_E(e^{j\phi})\right\}\right)^{-1} \quad \text{for } 0 \le \phi \le \pi \text{ and } 0 \le \theta \le 2\pi; \tag{3.6}$$

where $\bar{\sigma}(\Delta_{\min})$ represents the maximum magnitude of the smallest destabilizing $k_1$ or $k_2$; $\rho$ is the spectral radius; and $H_E(z^N) = (I - G_E(z^N))^{-1} G_E(z^N)$.

We are guaranteed that the system in Fig. 3.21 will remain stable as long as

$$\bar{\sigma}\begin{bmatrix} k_1 & 0 \\ 0 & k_2 \end{bmatrix} < \bar{\sigma}(\Delta_{\min}) \tag{3.7}$$

We are also guaranteed that when Eqn. (3.7) is violated, there exist values of $k_1$ and $k_2$ that destabilize the system in Fig. 3.21.

Equation (3.6) is straightforward to solve with a two dimensional search in $\phi$ and $\theta$. The results are given in Table 3.3. For comparison, the corresponding results for the design without the fictitious sensor noise are also given in Table 3.3 Notice that the addition of the fictitious noise increases the maximum singular value of the smallest destabilizing uncertainty by as much as 60%.

Even with the fictitious sensor noise, the robustness at the compensator inputs does not meet NASA's specification for a maximum singular value of 0.75. We could have improved the robustness at the

compensator output further by increasing the fictitious sensor noise level, but we chose not to do so because this simultaneously reduces the gain and phase margins at the compensator output.

## 3.6. CONCLUSIONS

The performance and robustness of the three $2^{nd}$ order compensators are nearly identical. All three stabilize the BACT wing at all 24 plant conditions and, with the exception of the robustness at the compensator input, satisfy all of NASA's specifications. From this perspective there is little reason to use the multirate designs over the single-rate design.

The real advantage of the multirate designs is that they allow the engineer to trade design simplicity for reductions in real-time computations or a reduction in hardware. The successive loop closures design trades a reduction in the number of computations for a more complex digital processor program. The multiplexed design trades one A/D converter for multiplexing hardware and a more complex digital processor program. Depending on the costs of the hardware, such trades might be very advantageous.

The $4^{th}$ order fault tolerant design, on the other hand, does not satisfy NASA robustness specifications. The compensator does, however, meet the robustness specifications to which it was designed. It stabilizes the BACT wing at all 24 operating point even if one of the accelerometers fails. This type of robustness - to a very specific perturbation - would be difficult to achieve using more common robustness improvement techniques such as Loop Transfer Recovery, but was straightforward to achieve using the multiple plant condition capability of our synthesis algorithm.

Blank

# 4. CONCLUSIONS AND RECOMMENDATIONS

## 4.1. CONCLUSIONS

The principle advantage of multirate control is that it gives the designer freedom to choose a sampling schedule which best utilizes the available hardware and software. In the flutter suppression system design, for example, we developed multirate controllers that provide performance comparable to a single-rate design, yet require either fewer real time multiplications per unit time to implement or require fewer A/D converters.

The disadvantage of multirate control is that this additional flexibility substantially increases the complexity of design and analysis over the single-rate case. Undoubtedly, the lack of good design and analysis tools has discouraged many from applying multirate control even when the situation may be ideal for a multirate design.

In this report we addressed the difficulty of multirate design and analysis by presenting a multirate design methodology. The methodology specifies a design approach and provides specific tools necessary to apply the approach to a practical problem. The tools are for modeling a multirate system, for synthesizing a multirate compensator which is robust to plant perturbations, and for analyzing the performance and robustness of a multirate system. The resulting methodology is powerful and straightforward to apply.

To demonstrate the methodology we applied it to design several multirate compensators for NASA's BACT wing. Those compensators satisfy the specified design specifications and illustrate some of the benefits of multirate control.

## 4.2. RECOMMENDATIONS FOR FUTURE RESEARCH

1) Our synthesis algorithm currently requires a stabilizing initial guess for the digital processor gains. Obtaining a stabilizing initial guess for those gains can be difficult, especially when the multiple plant conditions capability of the algorithm is used, because the initial guess must stabilize all plant conditions simultaneously. Eliminating this requirement would substantially improve the algorithm's versatility.

2) The singular value analysis of multirate systems leads directly to a structured singular value problem with repeated blocks. Calculating an exact solution to this problem is difficult for all but the simple tow parameter case. This is an area which needs further research.

Blank

# REFERENCES


1. Amit, N., and Powell J.D., "Optimal Control of Multirate Systems," *Proc. AIAA Guid. Contr. Conf.*, Albuquerque, NM, 1981.

2. Apostolakis, I.S. and Jordan, D., "Multirate system Performance Evaluation Using Singular Value Analysis," *1990 ACC*, pp.1502-1507.

3. Bennett, R.M., Eckstrom, C.V., Rivera, J.A.Jr., Dansberry, B.E., Farmer, M.G., and Durham, M.H., "The Benchmark Aeroelastic Models Program - Description and Highlights of Initial Results," NASA Tech. Memo. 104180, Dec. 1991

4. Berg, M.C., "Design of Multirate Digital Control Systems," Ph.D. Thesis, Stanford Univ., Stanford, CA, 1986.

5. Berg, M.C., Amit, N. and Powell, J.D., "Multirate Digital Control System Design," *IEEE Trans. Auto. Contr.*, Vol AC-33, Dec 1988, pp.1139-1150.

6. Berg, M.C., and Yang, G.S., "A New Algorithm for Multirate Digital Control Law Synthesis," *Proc. IEEE Conf. Decision Contr.*, Dec 1988, Austin, TX, pp. 1685-1690.

7. Berg, M.C. and Mason, G.S., "Multirate Sampled-Data Yaw-Damper and Modal Suppression System Design," Final Report for NASA Langley Research Grant NAG-1-1055, Feb. 1991.

8. Berg, M.C., Mason, G.S. and Yang, G.S., "A New Multirate Sampled-Data Control Law Structure and Synthesis Algorithm," *AIAA Journal of Guidance, Control and Dynamics*, Vol. 15, No. 5, 1992, pp. 1183-1191.

9. Boyd, S., and Doyle, J., "Comparison of peak and RMS gains for discrete-time systems," *Systems & Control Letters*, vol 9, 1987, pp. 1-6.

10. Boykin, W.H. and Frazier, B.D., "Analysis of Multiloop, Multirate Sampled-Data Systems," *AIAA Jour. Guid. Control & Dyn.*, Vol. 13, May 1975.

11. Dansberry, B.E., "Dynamic characteristics of a Benchmark Models Program Supercritical Wing," AIAA Paper No. 92-2368, April, 1992.

12. Dahleh, M.A., Voulgaris, P.G., and Valavani, L.S., "Optimal and Robust Controllers for Periodic and Multirate Systems," *IEEE Trans. Auto. Control*, Vol. 37, No 1., January 1992, pp. 90-99.

13. Doyle, J., "Analysis of Feedback systems with Structured Uncertainties," *IEE Proc.*, Vol 129, Pt. D, No. 6, Nov. 1982, pp. 243-250.

14. Doyle, J.C., and Stein, G., "Multivariable Feedback Design: Concepts for a Classical/Modern Synthesis," *IEEE Trans. Auto. Control*, Vol AC-26, Mo 1, Feb 1981, pp 4-16.

15. Durham, M.H., Keller, D.F., Bennett, R.M., Wieseman, C.D., "A Status Report on a Model for Benchmark Active Controls Testing," AIAA Paper No. 91-1011, April 1991.

16. Franklin, G.F., Powell, J. David, and Workman, M.L., *Digital Control of Dynamic Systems*, Addison-Wesley Pub. Co. 1990.

17. Glasson, D.P., "A New Technique for Multirate Digital Control Design and Sample Rate Selection," *AIAA Jour. Guid. Control & Dyn.*, Vol. 5, July-Aug. 1982.

18. Glasson, D.P., "Development and Application of Multirate Digital Control," *IEEE Control Systems Magazine*, Vol. 3, No. 4, 1983, pp. 2-8.

19. Kalman, R.E. and Bertram, J., "A Unified Approach to the Theory of Sampling Systems," *Journal of the Franklin Institute*, Vol 267, May 1957.

20. Kono, M., "Eigenvalue assignment in Linear Periodic Discrete-Time Systems," *Int. J. Control*, Vol. 32, No. 1, 1980, pp. 149-158.

21. Kranc, G.M. "Compensation of an Error Sampled System by a Multirate Controller," *Part II, AIEE Transactions*, Vol. 76, July 1957.

22. Kranc, G.M., "Input-Output Analysis of Multirate Feedback Systems," *IRE Trans. Auto. Control*, Vol. AC-3, Nov. 1957, pp. 21-28.

23. Kwakernaak, H. and Sivan, R., *Linear Optimal Control Systems*. New York, Wiley, 1972

24. Ly, U.L., "A Design Algorithm for Robust Low-Order Controllers." Ph.D. Thesis, Stanford Univ., Stanford, CA, 1982.

25. MacFarlane, A.G.J., "Return-Difference and Return-Ratio Matrices and Their Use in Analysis and Design of Multivariable Feedback Control Systems," *IEE Proc.*, Vol. 117, No. 10, Oct. 1970, pp.2037-2049.

26. Maciejowski, J.M., *Multivariable Feedback Design*, Addison-Wesley Publishing Company, Reading Mass. 1990.

27. Mason, G.S., "Multirate Compensator Synthesis and Analysis", Ph.D. Dissertation, Univ. Washington. 1993

28. Mason, G.S. and Berg, M.C., "Reduced Order Multirate Compensator Synthesis," *AIAA Jour. Guid. Contr. and Dynamics*, Vol 15, No. 3 May-June 1992, pp. 700-706.

29. Mason, G.S. and Berg, M.C., "Robustness Analysis of a Multirate Flutter Suppression System," *AIAA Journal of Guidance, Control and Dynamics*, Vol. 16, No. 5, 1993, pp. 992-926.

30. Mason, G.S. and Berg, M.C., "Multirate Flutter Suppression System for a Model Wing," accepted for publication in the *AIAA Journal of Guidance, Control and Dynamics*.

31. Meyer, R.A., and Burrus, C.S., "A Unified Analysis of Multirate and Periodically Time-Varying Digital Filters," *IEEE Trans. Circuits in Systems*, Vol. CAS-22, No. 3, March 1975, pp. 162-168.

32. Mukhopadhyay, V., "Digital Robust Control Law Synthesis Using Constrained Optimization," *AIAA Jour. Guid., Contr. and Dynamics*, Vol. 12, March-April 1989, pp. 175-181.

33. Mukhopadhyay, V., and Newsom, J.R., "A Multiloop System Statility Margin Study Using Matrix Singular Values," *AIAA Jour. Guid., Contr. and Dynamics*, Vol. 7, Sept-Oct 1984, pp. 582-587.

34. Mukhopadhyay, V., Newsom, J.R., and Abel, I., "A Method for Obtaining Reduced-Order Control Laws for High-Order Systems Using Optimization," NASA Tech. Paper 1876, August 1981.

35. Narigon, M.L., "Optimal Sample Policies for Multirate Digital Control," Ph.D. Thesis, Stanford Univ., Stanford, CA, 1991.

36. Packard, A., "What's New with MU: Structured Uncertainty in Multivariable Control," Ph.D. Dissertation, Univ. Cal. Berkley, 1988.

37. Safonov. M., and Doyle, J. C., "Minimizing Conservativeness of Robustness Singular Values," *Multivariable Control: New Concepts and Tools*, 1984, pp. 197-207

38. Safonov, M. G., "Stability Margins of Diagonally Perturbed Multivariable Feedback Systems," *IEE Proc.*, Vol. 129, Pt. D, No. 6, Nov. 1982, pp. 251-256.

39. Sivashankar, N. and Khargonekar, P. P., "Induced Norms for Sampled-Data Systems", *Automatica*, Vol. 28, No. 6, 1992, pp. 1267-1272.

40. Thompson, P. M., "Gain and Phase margins of Multirate sampled-data Systems," *International Journal of Automatic Control*, Vol. 4, No. 3, 1986, pp. 833-846.

41. Yang, G. S., "A generalized Synthesis Method for Multirate Feedback Control Systems," Ph. D. Dissertation, University of Washington, Seattle, Washington, 1988.

42. Zhu, G. and Skelton, R. E., "Robust Properties of Periodic Discrete and Multirate Systems," *IEEE Trans. Auto. Control*, Vol. 36, No. 5, May 1992, pp. 610-615.

43. Mason, G. S., Berg, M. C., and Mukhopadhyay, V., "Multirate Flutter Suppression System Design for the Benchmark Active Controls Technology Wing: *Part II : Methodology Application Software Toolbox*, NASA TM 2002-212129, December 2002.

Blank

# APPENDIX A. DESIGN RESULTS

Following are the state space matrices for the optimized flutter suppression system digital processors discussed in Section 3.0.

## A.1. SINGLE-RATE $2^{ND}$ ORDER

STP=BTP=0.02 sec; $N$=1. See Section 3.4.2.1 for a description of the sampling schedule.

$$\begin{bmatrix}\bar{z}_1(m+1,0)\\ \bar{z}_2(m+1,0)\end{bmatrix}=\begin{bmatrix}0 & 1\\ -0.61542 & 1.3562\end{bmatrix}\begin{bmatrix}\bar{z}_1(m,0)\\ \bar{z}_2(m,0)\end{bmatrix}+\begin{bmatrix}0 & -0.87258\\ 1 & -0.94601\end{bmatrix}\begin{bmatrix}\text{TE Accel}(m,0)\\ \text{LE Accel}(m,0)\end{bmatrix}$$

$$\text{CS Cmd}(m,0)=10^{-5}\begin{bmatrix}2.8302 & -13.621\end{bmatrix}\begin{bmatrix}\bar{z}_1(m,0)\\ \bar{z}_2(m,0)\end{bmatrix}$$

## A.2. MULTIRATE SUCCESSIVE LOOP CLOSURES

STP=0.02 sec; BTP=0.08 sec; $N$=4. See Section 3.4.2.2 for a description of the sampling schedule.

Update during first STP of the BTP:

$$\begin{bmatrix}\bar{z}_f(m,1)\\ \bar{z}_s(m+1,0)\end{bmatrix}=\begin{bmatrix}0.75673 & 0\\ 0 & -0.47672\end{bmatrix}\begin{bmatrix}\bar{z}_f(m,0)\\ \bar{z}_s(m,0)\end{bmatrix}+\begin{bmatrix}-1 & 0.37644\\ -10^{-4} & 0.53661\end{bmatrix}\begin{bmatrix}\text{TE Accel}(m,0)\\ \text{LE Accel}(m,0)\end{bmatrix}$$

$$\text{CS Cmd}(m,0)=10^{-4}\begin{bmatrix}2.35354 & -2.5338\end{bmatrix}\begin{bmatrix}\bar{z}_f(m,0)\\ \bar{z}_s(m,0)\end{bmatrix}$$

Update during second STP of the BTP:

$$\bar{z}_f(m,2)=0.75673\bar{z}_f(m,1)+\begin{bmatrix}-1 & 0.37644\end{bmatrix}\begin{bmatrix}\text{TE Accel}(m,1)\\ \text{LE Accel}(m,1)\end{bmatrix}$$

$$\text{CS Cmd}(m,1)=10^{-4}\begin{bmatrix}-2.5338 & 2.35354\end{bmatrix}\begin{bmatrix}\bar{z}_f(m,1)\\ \bar{z}_s(m,0)\end{bmatrix}$$

Update during third STP of the BTP:

$$\bar{z}_f(m,3)=0.75673\bar{z}_f(m,2)+\begin{bmatrix}-1 & 0.37644\end{bmatrix}\begin{bmatrix}\text{TE Accel}(m,2)\\ \text{LE Accel}(m,2)\end{bmatrix}$$

$$\text{CS Cmd}(m,2)=10^{-4}\begin{bmatrix}-2.5338 & 2.35354\end{bmatrix}\begin{bmatrix}\bar{z}_f(m,2)\\ \bar{z}_s(m,0)\end{bmatrix}$$

Update during fourth STP of the BTP:

$$\bar{z}_f(m+1,0) = 0.75673\bar{z}_f(m,3) + \begin{bmatrix} -1 & 0.37644 \end{bmatrix} \begin{bmatrix} \text{TE Accel}(m,3) \\ \text{LE Accel}(m,3) \end{bmatrix}$$

$$\text{CS Cmd}(m,3) = 10^{-4} \begin{bmatrix} -2.5338 & 2.35354 \end{bmatrix} \begin{bmatrix} \bar{z}_f(m,3) \\ \bar{z}_s(m,0) \end{bmatrix}$$

We assumed that $\bar{z}_S$ is updated during the first STP of the BTP, but it it can be updated during any STP of the BTP.

## A.3. MULTIRATE MULTIPLEXED INPUT

STP=0.02 sec; BTP=0.04 sec; $N$=2. See Section 3.4.2.3 for a description of the sampling schedule

Update during first STP of the BTP: Only the TE Accelerometer is sampled. The LE Accel value is held from the previous STP.

$$\begin{bmatrix} \bar{z}_1(m,1) \\ \bar{z}_2(m,1) \end{bmatrix} = \begin{bmatrix} 0 & 1 \\ -0.14712 & 0.88072 \end{bmatrix} \begin{bmatrix} \bar{z}_1(m,0) \\ \bar{z}_2(m,0) \end{bmatrix} + \begin{bmatrix} -1.3322 & 186.76 \\ -0.75421 & 136.42 \end{bmatrix} \begin{bmatrix} \text{TE Accel}(m,0) \\ \text{LE Accel}(m-1,1) \end{bmatrix}$$

$$\text{CS Cmd}(m,0) = 10^{-5} \begin{bmatrix} 8.6277 & -8.7583 \end{bmatrix} \begin{bmatrix} \bar{z}_1(m,0) \\ \bar{z}_2(m,0) \end{bmatrix}$$

Update during second STP of the BTP: Only the LE Accelerometer is sampled.The TE Accel value is held from the previous STP.

$$\begin{bmatrix} \bar{z}_1(m+1,0) \\ \bar{z}_2(m+1,0) \end{bmatrix} = \begin{bmatrix} 0 & 1 \\ -2.3304 & 3.7275 \end{bmatrix} \begin{bmatrix} \bar{z}_1(m,1) \\ \bar{z}_2(m,1) \end{bmatrix} + \begin{bmatrix} -2.5371 & -191.09 \\ -0.28724 & -189.04 \end{bmatrix} \begin{bmatrix} \text{TE Accel}(m,0) \\ \text{LE Accel}(m,1) \end{bmatrix}$$

$$\text{CS Cmd}(m,1) = 10^{-4} \begin{bmatrix} 3.7645 & -4.6910 \end{bmatrix} \begin{bmatrix} \bar{z}_1(m,1) \\ \bar{z}_2(m,1) \end{bmatrix}$$

## A.4. SINGLE-RATE FAULT TOLERANT

STP=0.005 sec; BTP=0.005 sec; $N$=1. See Section 3.4.2.4 for a description of the sampling schedule.

$$\begin{bmatrix} \bar{z}_1(m+1,0) \\ \bar{z}_2(m+1,0) \\ \bar{z}_3(m+1,0) \\ \bar{z}_4(m+1,0) \end{bmatrix} = \begin{bmatrix} 0 & 1 & 0 & 0 \\ 0 & 0 & 1 & 0 \\ 0 & 0 & 0 & 1 \\ -0.48177 & 2.4151 & -4.3750 & 3.4415 \end{bmatrix} \begin{bmatrix} \bar{z}_1(m,0) \\ \bar{z}_2(m,0) \\ \bar{z}_3(m,0) \\ \bar{z}_4(m,0) \end{bmatrix}$$

$$+10^{-5} \begin{bmatrix} 4.2073 & 6.4437 \\ -0.06264 & 1.3823 \\ -2.1575 & -1.1393 \\ -3.1600 & -2.3865 \end{bmatrix} \begin{bmatrix} \text{TE Accel}(m,0) \\ \text{LE Accel}(m,0) \end{bmatrix}$$

$$\text{CS Cmd}(m,0) = \begin{bmatrix} 1 & 0 & 0 & 0 \end{bmatrix} \begin{bmatrix} \bar{z}_1(m,0) \\ \bar{z}_2(m,0) \\ \bar{z}_3(m,0) \\ \bar{z}_4(m,0) \end{bmatrix}$$

Blank

# APPENDIX B. M-FILES USED TO DEFINE THE FLUTTER SUPPRESSION SYSTEM SYNTHESIS PROBLEM

## B.1. PAPA ABCD

*Format*: **[am, bm, cm, dm, vm]=PAPAabcd(fname, rolloff, form)**

*Description*: Creates state space matrices defining the PAPA wing at operating point specified in **fname** such that

$$\dot{x} = \mathbf{am}x + \mathbf{bm}u$$
$$y = \mathbf{cm}x + \mathbf{dm}u$$

where $y = \left\{ \begin{array}{l} \text{plunge} \\ \text{pitch} \\ \text{plunge rate} \\ \text{pitch rate} \\ \text{TE accelerometer} \\ \text{LE accelerometer} \\ \text{command to actuator} \\ \text{CS control surface} \\ \text{CS control surface rate} \\ \text{CS control surface accel} \\ \text{mode 1} \\ \text{mode 2} \\ \text{mode 3} \\ \text{mode 4} \end{array} \right\}$ and $u = \left\{ \begin{array}{l} \text{CS command} \\ \text{Dryden filter input} \end{array} \right\}$

*Inputs*: **fname** text variable containing the name of the operating point of interest. e.g. 'freon_m5_q75'. **fname** must have the same name as the file which contains the data

**rolloff** frequency in rad/sec of first order anti-aliasing roll-off at the sensors. The filter has the form

$$y_{filtered} = \frac{\mathbf{rolloff}}{s+\mathbf{rolloff}} y_{unfiltered}$$

**form** indicates the desired form

if **form** = 0 : **am, bm, cm, dm** is unchanged from original data
1 : **am, bm, cm, dm** is block diagonal
2 : **am, bm, cm, dm** is block diagonal with scaled states and outputs

*Outputs*: **am, bm, cm, dm** state space description of the plant

**vm** transformation matrix used to obtain modal form

### B.2. FSSCOMP

*Format*: [**cmp**, **sz**, **su**, **sy**, **stp**, **stppbtp**]=**FSScomp**(**ctype**)

*Description*: Generates the digital processor gain matrices and sampling schedule description for the four compensator described in Section 3.

*Inputs*: **ctype** specifies the desired compensator

if **ctype** = 'sr' then **FSScmp** returns a description of the $2^{nd}$ order Single-Rate design

'mrslc' then **FSScmp** returns a description of the Multirate Successive Loop Closure design

'mrmi' then **FSScmp** returns a description of the Multirate w/ Multiplexed Input design

**'srft** then **FSScmp** returns a description of the Single-Rate Fault Tolerant design

*Outputs*: **cmp**, **sz**, **su**, **sy**, **stp**, **stppbtp** a description of the compensator used by the synthesis algorithm. See Ref. 43 (NASATM 2002-212129).

### B.3. MROPT_SR OR MRMI

*Format*: **mropt_srORmrmi**

*Description*: Defines the input data for the $2^{nd}$ order single-rate compensator or multirate compensator with multiplexed inputs. The user needs to comment and uncomment three lines to switch between the SR and the MRMI design. These are indicated in the text of the script.

*Inputs*: none

*Outputs*: Outputs to global variables used by optimization routine and defined in Section 3.3 of Ref. 43 (NASATM 2002-212129).

### B.4. MROPT_MRSLC

*Format*: **mropt_mrslc**

*Description*: Defines the input data for the multirate compensator with successive loop closure form.

*Inputs*: none

*Outputs*: Outputs to global variables used by optimization routine and defined in Section 3.3 of Ref. 43 (NASATM 2002-212129).

### B.5. MROPT_SRFT

*Format*: **mropt_srft**

*Description*: Defines the input data for the single-rate fault tolerant compensator.

*Inputs*: none

*Outputs*: Outputs to global variables used by optimization routine and defined in Section 3.3 of Ref. 43 (NASATM 2002-212129).

# REPORT DOCUMENTATION PAGE

*Form Approved*
*OMB No. 0704-0188*



| 1. REPORT DATE *(DD-MM-YYYY)* | 2. REPORT TYPE | 3. DATES COVERED *(From - To)* |
|---|---|---|
| 12-2002 | Technical Memorandum | |

**4. TITLE AND SUBTITLE**

Multirate Flutter Suppression System Design for the Benchmark Active Controls Technology Wing
*Part I: Theory and Design Procedure*

**5a. CONTRACT NUMBER**

**5b. GRANT NUMBER**

**5c. PROGRAM ELEMENT NUMBER**

**6. AUTHOR(S)**

Mason, Gregory S.; Berg, Martin C.; and Mukhopadhyay, V.

**5d. PROJECT NUMBER**

**5e. TASK NUMBER**

**5f. WORK UNIT NUMBER**

706-17-51-03

**7. PERFORMING ORGANIZATION NAME(S) AND ADDRESS(ES)**

NASA Langley Research Center
Hampton, VA 23681-2199

**8. PERFORMING ORGANIZATION REPORT NUMBER**

L-18248

**9. SPONSORING/MONITORING AGENCY NAME(S) AND ADDRESS(ES)**

National Aeronautics and Space Administration
Washington, DC 20546-0001

**10. SPONSOR/MONITOR'S ACRONYM(S)**

NASA

**11. SPONSOR/MONITOR'S REPORT NUMBER(S)**

NASA/TM-2002-212128

**12. DISTRIBUTION/AVAILABILITY STATEMENT**

Unclassified - Unlimited
Subject Category 63
Availability: NASA CASI (301) 621-0390 Distribution: Nonstandard

**13. SUPPLEMENTARY NOTES**

An electronic version can be found at http://techreports.larc.nasa.gov/ltrs/ or http://techreports.larc.nasa.gov/cgi-bin/NTRS

**14. ABSTRACT**

To study the effectiveness of various control system design methodologies, the NASA Langley Research Center initiated the Benchmark Active Controls Project. In this project, the various methodologies were applied to design a flutter suppression system for the Benchmark Active Controls Technology (BACT) Wing. This report describes a project at the University of Washington to design a multirate suppression system for the BACT wing. The objective of the project was two fold. First, to develop a methodology for designing robust multirate compensators, and second, to demonstrate the methodology by applying it to the design of a multirate flutter suppression system for the BACT wing.

**15. SUBJECT TERMS**

Cybernetics; Digital Control Systems; Multirate sampling; Flutter suppression; Control law design and optimization; Metlab toolbox

| 16. SECURITY CLASSIFICATION OF: | | | 17. LIMITATION OF ABSTRACT | 18. NUMBER OF PAGES | 19a. NAME OF RESPONSIBLE PERSON |
|---|---|---|---|---|---|
| a. REPORT | b. ABSTRACT | c. THIS PAGE | | | STI Help Desk (email: help@sti.nasa.gov) |
| | | | | | 19b. TELEPHONE NUMBER *(Include area code)* |
| U | U | U | UU | 55 | (301) 621-0390 |